

1 Subsurface warming of the West Antarctic continental 2 shelf linked to El Niño-Southern Oscillation

3 **Maurice F. Huguenin^{1,2}, Ryan M. Holmes³, Paul Spence^{4,5}, and Matthew H.
4 England²**

5 ¹Climate Change Research Centre and ARC Centre of Excellence in Climate Extremes, University of New
6 South Wales, Sydney, New South Wales, Australia

7 ²Centre for Marine Science and Innovation and ARC Australian Centre for Excellence in Antarctic
8 Science, University of New South Wales, Sydney, New South Wales, Australia

9 ³School of Geosciences, University of Sydney and Australian Bureau of Meteorology, Sydney, New South
10 Wales, Australia

11 ⁴ARC Australian Centre for Excellence in Antarctic Science and Institute for Marine and Antarctic
12 Studies, University of Tasmania, Tasmania, Australia

13 ⁵Australian Antarctic Partnership Program, University of Tasmania, Tasmania, Australia

14 Key Points:

- 15 • Ocean-sea ice model simulations of El Niño and La Niña events illustrate how they
modulate West Antarctic shelf temperatures
- 16 • El Niño weakens coastal easterlies, reduces on-shelf Ekman flow of cold waters, in-
creasing cross-shelf transport of warm Circumpolar Deep Water
- 17 • The La Niña shelf circulation response is largely opposite and reduces cross-shelf
transport of warm Circumpolar Deep Water

Abstract

Recent observations suggest that El Niño–Southern Oscillation (ENSO) impacts basal melting of West Antarctic ice shelves, yet sparse ocean observations limit our understanding of the associated processes. Here we investigate how ENSO events modulate subsurface West Antarctic shelf temperatures using high-resolution global ocean-sea ice model simulations. During El Niño, the subsurface shelf warming between 150 m and the shelf bottom can be up to 0.5°C in front of ice shelves. This warming arises from a weaker Amundsen Sea Low (ASL) and weaker coastal easterlies that reduce on-shelf Ekman transport of cold surface waters, enabling enhanced transport of warm Circumpolar Deep Water (CDW) onto the shelf. A largely opposite response occurs during La Niña, with a stronger ASL and stronger Ekman transport that results in less cross-shelf CDW transport and cooling in the subsurface. These findings have implications for interpreting basal melting on interannual and decadal time-scales in West Antarctica.

1 Plain language summary

El Niño-Southern Oscillation (ENSO) is the Earth's dominant year-to-year climate variation. The impacts of its two phases, El Niño and La Niña, extend from the tropics to Antarctica through atmospheric waves. Past studies have suggested that West Antarctic ice shelves melt more during El Niño because of warmer ocean waters at the ice shelf bases. However, oceanic changes during El Niño, which lead to warmer shelf water near the ice, remain difficult to isolate. That is because ENSO is only one of many drivers that impact shelf water temperatures. In this work, we simulate isolated ENSO events using an ocean circulation model. We show that during El Niño, the on-shelf flow of cold surface waters in West Antarctic, driven by coastal easterly winds, is reduced because the winds weaken. To balance out this mass deficit at the surface, more warm Circumpolar Deep Water (CDW) flows onto the continental shelf below. During La Niña, we see a largely opposite response. Stronger coastal easterlies increase the on-shelf flow of cold surface waters and less CDW is flowing onto the shelf. Our results show the link between ENSO and mass loss of the West Antarctic ice shelves and ice sheet.

49 2 Introduction

50 Over recent decades, mass loss from the West Antarctic ice sheet has accelerated (e.g.,
 51 Scambos et al. (2017); Shepherd et al. (2018); Rignot et al. (2019)). This occurs primarily
 52 via basal melting induced by warm Circumpolar Deep Water (CDW) intruding into ice
 53 shelf cavities (Pritchard et al., 2012; Wåhlin et al., 2013; Jenkins et al., 2016; Kimura
 54 et al., 2017; Tamsitt et al., 2021; Assmann et al., 2013), impacting the buttressing and
 55 stability of the ice shelves (Gudmundsson, 2013; Fürst et al., 2016; Gudmundsson et al.,
 56 2019), causing large-scale calving (Greene et al., 2022) and contributing to rapid sea level
 57 rise (Naughten et al., 2023). Superimposed on decadal-scale ocean warming and associated
 58 basal melting (Schmidtko et al., 2014) is warming induced by internal climate variability.
 59 A better understanding of the impact of different modes of climate variability on the West
 60 Antarctic region is needed not only to separate the forced anthropogenic signal from natural
 61 variability but also because major climate modes may change in the future (Cai et al., 2014,
 62 2015, 2021; Goyal, Sen Gupta, et al., 2021; McGregor et al., 2022).

63 On decadal time scales, the observed shelf temperature variability in the Amundsen
 64 and Bellingshausen Seas is dominated by tropical Pacific climate variability via the Inter-
 65 decadal Pacific Oscillation (IPO, Dutrieux et al. (2014); Jenkins et al. (2018); Steig et al.
 66 (2012)). This climate mode impacts shelf temperatures through atmospheric teleconnec-
 67 tions, modifies surface buoyancy fluxes over the shelf (St-Laurent et al., 2015; Webber et
 68 al., 2017), modulates the depth of on-shelf isopycnals (Silvano et al., 2022) and also impacts
 69 the shelf-break undercurrent and its ability to bring warm CDW onto the shelf (Dotto et
 70 al., 2022; Kim et al., 2021; Kimura et al., 2017; Silvano et al., 2022; Thoma et al., 2008).

71 The most dominant mode of interannual climate variability is El Niño-Southern Oscil-
 72 lation (ENSO), and it is known to impact the atmospheric circulation in West Antarctica
 73 through its teleconnection to the Amundsen Sea (e.g., Karoly (1989); Hoskins and Ambrizzi
 74 (1993); Turner (2004); Lachlan-Cope and Connolley (2006); Fogt and Bromwich (2006);
 75 Raphael et al. (2016)). Recent satellite records of the West Antarctic ice shelves have
 76 shown that during El Niño, snow fall increases the height of the ice shelves but their overall
 77 mass decreases through basal melting (Paolo et al., 2018). This mechanism is supported by
 78 a modelling study highlighting how changes in the Amundsen Sea Low (ASL) affect surface
 79 heat fluxes and warming on the Bellingshausen Sea shelf (Oelerich et al., 2022). While these
 80 studies find that atmospheric variability associated with ENSO impacts West Antarctic ice
 81 shelves, they have not examined the isolated ocean dynamics driving these changes in detail.
 82 ENSO can also be thought of as a high-frequency mode of the IPO, with El Niño (IPO^+)
 83 and La Niña (IPO^-) teleconnections to Antarctica highlighting similar spatial anomalies.
 84 Thus, interannually-forced shelf temperature changes also have relevance to decadal Pacific
 85 forcing of Antarctic temperature variability.

86 The ENSO signal on the West Antarctic shelf (Fig. 1a) is difficult to identify as it
 87 can be masked by the Southern Annular Mode (SAM, Marshall (2003); Martinson et al.
 88 (2008); C. Walker and Gardner (2017)), zonal-wave 3 variations (Goyal, Jucker, et al., 2021;
 89 Goyal et al., 2022), coastally trapped Kelvin waves (Webb et al., 2022) and higher frequency
 90 variability, such as storm systems. Because of this difficulty to isolate the ENSO signal, its
 91 impacts on West Antarctica are less well understood (Jenkins et al., 2018). Research cruise
 92 and mooring data are sparse outside of the Peninsula region, with sea ice and icebergs making
 93 it challenging to obtain reliable observations (Heywood et al., 2016; Boehme & Rosso, 2021).
 94 Using coupled climate models to examine the impact of ENSO teleconnections on Antarctic
 95 shelf ocean behaviour remains difficult due to their biases in the shelf temperature structure
 96 (Heuzé et al., 2013; Heuzé, 2021; Purich & England, 2021; Li et al., 2023) and their lower
 97 ocean model resolution. However, West Antarctica is one of the most sampled Antarctic
 98 areas, and many studies (e.g., S. S. Jacobs et al. (2011); Dutrieux et al. (2014); Jenkins et al.
 99 (2018)) provide an overview of the observed interannual shelf temperature variability from
 100 combined climate modes in the Amundsen Sea since the 1990s. Here, we explore how isolated

101 atmospheric ENSO teleconnections impact the West Antarctic shelf ocean circulation and
 102 heat content using high-resolution global ocean-sea ice model simulations.

103 3 Methods

104 3.1 The ocean-sea ice model and experimental design

105 We use the global ocean-sea ice model ACCESS-OM2 (Kiss et al., 2020) with an eddy-
 106 rich horizontal resolution of $1/10^\circ$ (3.2 km at 73°S) and 75 z* vertical levels (47 levels in the
 107 upper 1000 m). ACCESS-OM2 combines the MOM5.1 ocean model (Griffies, 2012) and the
 108 CICE5.1.2 sea ice model (Hunke et al., 2015), and it is forced by atmospheric fields from
 109 the JRA55-do version 1.3 data set (Tsujino et al., 2018). See the Supporting Information
 110 for a more detailed model description as well as evaluation of model skill and circulation in
 111 West Antarctica.

112 The model is initialised from World Ocean Atlas 2013 v2 conditions (Locarnini et al.,
 113 2013) and spun-up using repeat cycles of the 1990–91 forcing for 245 years (K. Stewart et al.,
 114 2020). This 1990–91 period was chosen for the control experiment as it has relatively neutral
 115 conditions in SAM and ENSO (K. Stewart et al., 2020). Our experiments are formulated by
 116 adding composite mean atmospheric anomaly fields from four strong El Niño and four strong
 117 La Niña events (which capture the strongest teleconnections to the West Antarctic region) to
 118 the repeat-year baseline. This anomalous forcing is applied as time-constant spatial patterns
 119 multiplied by time series that correspond to the evolution of eastern equatorial Pacific sea
 120 surface temperatures (SSTs). This approach was taken as an analysis of the full evolution
 121 of the ENSO events in Fig. 1a would not have isolated its signal from other types of internal
 122 climate variability.

123 The spatial patterns for all forcing fields are constructed as the mean anomalies during
 124 the peak of the ENSO events six months on either side of the peak amplitude (Fig. 1b, c and
 125 Fig. S1, S2). We use this method for all ten input fields, including 10 m specific humidity,
 126 surface air temperature, zonal and meridional wind speed as well as SLP and surface rain-
 127 and snowfall, runoff, downward long- and shortwave radiation (Fig. S3, S4). The spatial
 128 pattern of SLP anomalies during ENSO is an opposite sign teleconnection, although La
 129 Niña anomalies show a peak signature further west and broader in extent. This is because
 130 during La Niña, convective heating anomalies excite a Rossby wave train from the western
 131 rather than the central equatorial Pacific (Chiodi & Harrison, 2015), and SLP anomalies
 132 are more elongated because the ASL centre during the 1988/89 La Niña was located further
 133 west than during the other three events (Fig. S2b). While using spatial anomalies from
 134 composite ENSO events can also incorporate anomalies associated with SAM variability,
 135 the SAM signature appears to be small during these events (Fig. S5).

136 The spatial patterns are scaled by corresponding composite time series throughout the
 137 events (Fig. 1d, e). The time series are constructed by taking the mean Niño 3.4 index
 138 during the four strong El Niño/La Niña events, centered around the peak amplitude (bold
 139 black line, Fig. 1d, e). For the La Niña simulation, we extend the time series 12 months
 140 back as most strong La Niña events follow immediately after El Niño, and our goal is to
 141 keep this memory in case it is relevant to the La Niña response. Each time series has been
 142 normalised by matching the amplitude to the mean Niño 3.4 SST anomalies during the peak
 143 of the four strong events (the time series were divided by 1.56°C for El Niño and 1.33°C for
 144 La Niña, Fig. S6).

145 3.2 The West Antarctic subsurface heat budget

146 To investigate the drivers of West Antarctic shelf temperature changes during ENSO,
 147 we consider the subsurface heat budget between 100 m and the shelf bottom over a region
 148 bounded by 150°W – 60°W and the 1000 m isobath to the north (hereafter the West Antarctic

shelf region). The change in heat content with time is defined as the sum of the advective heat transport convergence, vertical mixing across 100 m and radiative fluxes penetrating below 100 m (which are negligible). These terms are all calculated online in the model.

The heat transport convergence can be decomposed into its vertical, along-shelf and cross-shelf components, and we do these calculations offline using monthly averages. These offline flux calculations miss sub-monthly variations, mainly due to mesoscale eddies which can act to advect heat onto the shelf to ice shelf cavities (St-Laurent et al., 2013; Friedrichs et al., 2022; Foppert et al., 2021), but the sub-monthly variations are captured by the computed uncertainty limits in our heat fluxes (elaborated below). The vertical heat flux is calculated across 100 m depth and the along-shelf heat flux is calculated as the sum of the heat fluxes across the shelf transects at 150°W and 60°W. We calculate the remaining component, the cross-shelf component, which corresponds to the heat flux across the 1000 m isobath, by residual. We have checked, using online calculations, that both the vertical and along-shelf heat fluxes are of much smaller magnitude and that inferring the cross-shelf heat flux as a residual is an appropriate choice.

Due to the potential for non-zero anomalous mass fluxes, separating the heat transport convergence into components introduces an uncertainty for each component associated with an arbitrary reference temperature (Holmes et al., 2019; Forget & Ferreira, 2019; Huguenin et al., 2022). Here, we estimate uncertainty ranges of the individual anomalous heat flux components by multiplying the change in the volume flux of each component by the ± 1 standard deviation range (assuming the values follow a normal distribution) of the climatological temperature across the volume considered in the heat budget. Effectively, this approximates the possible range of temperatures at which the anomalous volume flux could be returned (see the Supporting Information in Holmes et al. (2019)).

4 Shelf temperature response

We first analyse the spatial distribution of ENSO-associated temperature anomalies during the peak of the event in austral summer. Around the Pine Island Bay (at 101°W) and along the Peninsula, depth-averaged shelf warming reaches up to 0.5°C (Fig. 2a), and it is this localised warming that is important for melting of grounded ice shelves. This is also the region where mass loss of the West Antarctic ice shelves and ice sheet has experienced the highest acceleration over recent years (Paolo et al., 2015; Rignot et al., 2019). Despite overall shelf water warming during El Niño, local areas also experience subsurface cooling, predominantly along the outer shelf region, likely caused by eddies and mixed-layer responses. During the peak of La Niña, subsurface cooling occurs with a similar magnitude and in similar regions as warming during El Niño. As the atmospheric anomalies are strongest over West Antarctica, shelf temperatures outside of this region are minimally impacted and not shown here.

El Niño-induced warming peaks at around 200 m depth and 180 km south of the shelf break in both the Amundsen-Bellingshausen Sea and in the Peninsula region, extending to the shelf bottom (Fig. 2c, e). Warming anomalies averaged along-shelf in these regions reach 0.5°C, although mean vertical shifts in isopycnals and isotherms are relatively small. Many ice shelves in this region have grounding lines at depths of 500 m or more (Davis et al., 2023). Thus, the warming signal we simulate in response to El Niño has the potential to cause increased basal melting of the ice shelves.

5 Driving Mechanisms

5.1 El Niño warming

The subsurface West Antarctic shelf warming persists for almost one year after the peak of the El Niño event, and even throughout the six-month extension of the simulation

where forcing returns to the climatological state (Fig. 3a). This is consistent with Tamsitt et al. (2021) who highlighted the more than one-year-long residence time of warm waters on the West Antarctic shelf. To explore the mechanisms driving this warming, we now analyse the ocean heat budget over West Antarctica.

The build-up of heat during El Niño occurs before the event peaks (black line, Fig. 3e). The dominant advective heat flux component, that almost always dominates the heat budget, is the cross-shelf heat flux (red line and red shaded interval, Fig. 3e). This heat flux is associated with the cross-shelf transport of warm CDW and is the result of ENSO-related atmospheric anomalies over the shelf region. During the build-up phase of El Niño, the ASL and coastal easterly surface winds weaken around West Antarctica (Fig. 1b). The reduced winds decrease the cross-shelf Ekman transport of cold surface waters (Fig. 3c), causing a tilt in sea level on and off the shelf. Various possible mechanisms can then result in cross-shelf flow of warm CDW that typically resides at mid-depth layers off the shelf break: (1) heat advected onto the shelf by the bottom Ekman response that results from flow down the barotropic pressure gradient established by the sea level anomaly (Wåhlin et al., 2012; Spence et al., 2017), (2) baroclinic adjustment (shoaling of the isopycnals) from the pressure gradient bringing more warm water up onto the shelf (Spence et al., 2014; Dotto et al., 2022), (3) in the Amundsen Sea, anomalous cross-shelf heat transport associated with strengthening of the undercurrent and interaction with topography there (Nakayama et al., 2013; Dotto et al., 2022; Kimura et al., 2017; Silvano et al., 2022), and (4) heat transported towards the continent by eddies (A. L. Stewart & Thompson, 2015). Heat transport via CDW towards the shelf on ENSO time scales thus varies with Ekman transport. While the cross-shelf heat transport dominates in our simulation, the vertical advective heat flux, the vertical mixing across 100 m depth, and the surface heat/buoyancy fluxes are negligible (Fig. S8a).

A reversal of the warming tendency on the shelf is initiated about six months after the peak of the El Niño (Fig. 3a). The return to climatological shelf temperatures is a much slower process than the warming, even though the atmospheric anomalies are largely symmetric in the increasing and decreasing stages of the simulation. As easterly winds return back to climatological conditions, anomalous heat is slowly discharged across the shelf northwards and to a small extent across the transects at 150°W and 60°W (Fig. 3e and Fig. S8a). Warm shelf temperatures persist beyond month 18 (Fig. 3a). This occurs despite El Niño slowly transitioning into a negative La Niña-like state with stronger easterly winds on the shelf (Fig. 1b,d).

5.2 La Niña cooling

During La Niña, the ASL strengthens and West Antarctic coastal easterlies increase (Fig. 1c). This increases on-shelf Ekman transport of cold surface waters onto the shelf (Fig. 3d), establishing a pressure gradient and reducing transport of CDW onto the shelf. At the same time, mixing of cooler water across the 100 m depth level is enhanced. This is likely caused by changes in the vertical stability under different signs of surface flux anomalies, by increased sea ice growth (Fig. S9d) and convection because the stronger easterlies have the potential to create larger polynyas (openings within the ice cover) that impact buoyancy fluxes and the flow of warm water onto the shelf (Moorman et al., 2023). This might also be a contributing factor why cooling during La Niña is larger than warming during El Niño.

The shelf temperature cooling during La Niña persists throughout the full simulation (Fig. 3b). Overall cooling rates are much larger than warming rates during the El Niño simulation (months 20-24, Fig. 3f), despite the La Niña following the tail end of an El Niño. La Niña also often re-intensifies the following year (Okumura & Deser, 2010), a feature that can be seen in our model forcing (Fig. 1e), and thus subsurface West Antarctic cooling on the shelf intensifies again in month 28 of the simulation (Fig. 3f). The uncertainties associated with the vertical advective heat flux are larger than during El Niño because

248 Ekman-induced vertical downwelling of cool surface waters is enhanced. Subsurface cooling
 249 continues through to the end of the La Niña and during the 6-month extension of the
 250 simulation with climatological forcing (Fig. 3f).

251 **6 Discussion and Conclusions**

252 ENSO shows considerable event-to-event variability with differing teleconnections to the
 253 Amundsen Sea (e.g., Fig. S1, S2). While the wind-driven mechanisms presented here will be
 254 consistent across events, we expect the strongest shelf temperature impacts during events
 255 when West Antarctic wind anomalies are well-aligned to the shelf break geometry (Fig.
 256 S1d, S2d), for example during the 2011-12 La Niña when observations measured a notably
 257 cool Amundsen Sea state (Jenkins et al., 2018) and reduced Pine Island ice shelf melting
 258 (Dutrieux et al., 2014). While we can equally expect a strong warming response during the
 259 ensuing 2015-16 El Niño, observations still showed persistently cool shelf conditions until
 260 2016 (Jenkins et al., 2018), possibly because this ENSO event coincided with a positive phase
 261 of the SAM (Vera & Osman, 2018) that would tend to offset the ENSO warming effect and
 262 reduce the strength of the atmospheric teleconnection to the Amundsen Sea region (Fogt et
 263 al., 2011; Paolo et al., 2015). Another possible factor could be that the shelf circulation and
 264 ice shelves react more strongly on decadal time scales, so that longer-term variability such
 265 as that due to the IPO dominates the 2015-16 El Niño response. This is also suggested by
 266 observations (e.g., Fig. 5 in Jenkins et al. (2018)).

267 When considering not just the ENSO impact but the full climate variability, Oelerich et
 268 al. (2022) find that when the ASL strengthens, Bellingshausen Sea subsurface temperatures
 269 below 300 m decrease and an anomalous northward heat transport takes place. This is
 270 consistent with the mechanisms presented here during La Niña, when a strengthening of
 271 the ASL cools the Bellingshausen Sea shelf region (Fig. 2b), and this cooling is linked to
 272 weaker cross-shelf advective heat fluxes in the CDW layer (Fig. 3f).

273 Future climate change simulations predict an increase in the variability and amplitude
 274 of ENSO events by 2100 (Wang et al., 2022; Cai et al., 2021), and also suggest a
 275 net West Antarctic shelf warming impact because El Niño-induced warming appears to be
 276 overall greater than the La Niña-induced cooling (Dommegget et al., 2013; Cai et al., 2023).
 277 However, this past work by Cai et al. (2023) relies on coarse-resolution models which may
 278 overestimate future ENSO-related teleconnections due to West Antarctic warm biases in
 279 these models (Heuzé (2021); Li et al. (2023) and Fig. 2 in Purich and England (2021)).
 280 Despite these known CMIP6 shelf water biases, our model suggests similar rectification ef-
 281 fects as in Cai et al. (2023), because in our simulation, the shelf warms for longer than it
 282 cools over one strong ENSO cycle (Fig. S10b). However, key to this net effect is also the
 283 amplitude of the warming, with basal melt rates responding more rapidly to increases than
 284 to decreases in advective heat fluxes (Kimura et al., 2017).

285 We have investigated how atmospheric ENSO teleconnections modulate West Antarctic
 286 shelf temperatures. During El Niño, the ASL and coastal easterlies weaken (Fig. 4a).
 287 Accordingly, on-shelf Ekman transport of cold surface water is reduced and this enhances
 288 cross-shelf transport of warm CDW via the establishment of a pressure gradient. During La
 289 Niña, we find a largely opposite response with a stronger ASL, stronger surface easterlies
 290 and increased on-shelf flow of cold surface waters that reduces cross-shelf transport of warm
 291 CDW (Fig. 4b). Limitations in our results arise from the use of a single model, the weak
 292 undercurrent and a shallower thermocline in the Amundsen Sea as well as a shelf salinity
 293 bias in the Peninsula region. Given the resemblance of El Niño and La Niña to IPO⁺ and
 294 IPO⁻ phases (Fig. S11, S12), these mechanisms are likely to also play out on decadal time
 295 scales, although modulated by other factors (Silvano et al., 2022). The results highlight the
 296 need to reconcile interannual to decadal climate variability alongside future climate change
 297 in this vital sector of the Antarctic margin.

298 7 Open Research

299 The scripts to create the perturbation experiment forcing, the analysis scripts and the
300 data to recreate the figures in this study have been deposited online and published under
301 Huguenin (2023a, 2023b). A small temperature snapshot of the full model data is also avail-
302 able in this data base. Upon acceptance of this manuscript, the full model simulation data
303 will be stored on the Consortium for Ocean-Sea Ice Modelling in Australia data collection
304 website (COSIMA, 2020). The marine mammal data from Roquet et al. (2013); Treasure
305 et al. (2017) were collected and made freely available by the International MEOP Conso-
306 rium and the national programs that contribute to it ([https://www.meop.net/database/
307 download-the-data.html](https://www.meop.net/database/download-the-data.html)). The ACCESS-OM2 model source code from Kiss et al. (2020)
308 is available at <https://github.com/COSIMA/access-om2>. The Pine Island mooring data
309 is available from Webber et al. (2017); S. Jacobs and Huber (2016).

310 8 Acknowledgments

311 We thank Adele Morrison, Georgina Harmer, Ole Rieke, Shang-Ping Xie, John Fasullo,
312 Zhi Li, Famille Huguenin and two reviewers for their valuable input. We thank the Conso-
313 rium for Ocean-Sea Ice Modelling in Australia (COSIMA; <https://cosima.org.au/>) for
314 their technical help and continued development of ACCESS-OM2. The simulations were con-
315 ducted with resources and services from the National Computational Infrastructure which
316 is supported by the Australian Government. M. F. H. was supported by a University of
317 New South Wales Scientia PhD scholarship, the Australian Research Council (ARC) Centre
318 of Excellence for Climate Extremes (ARC Grant No. CE170100023) and is now supported
319 by the Centre for Excellence in Antarctic Studies (ARC Grant No. SR200100008). R. M.
320 H. was supported by ARC grant DE21010004, P. S. by ARC grant FT190100413, and P. S.
321 and M. H. E. are supported by ARC Grant No. SR200100008.

322 9 Competing Interests

323 The authors declare no competing interests.

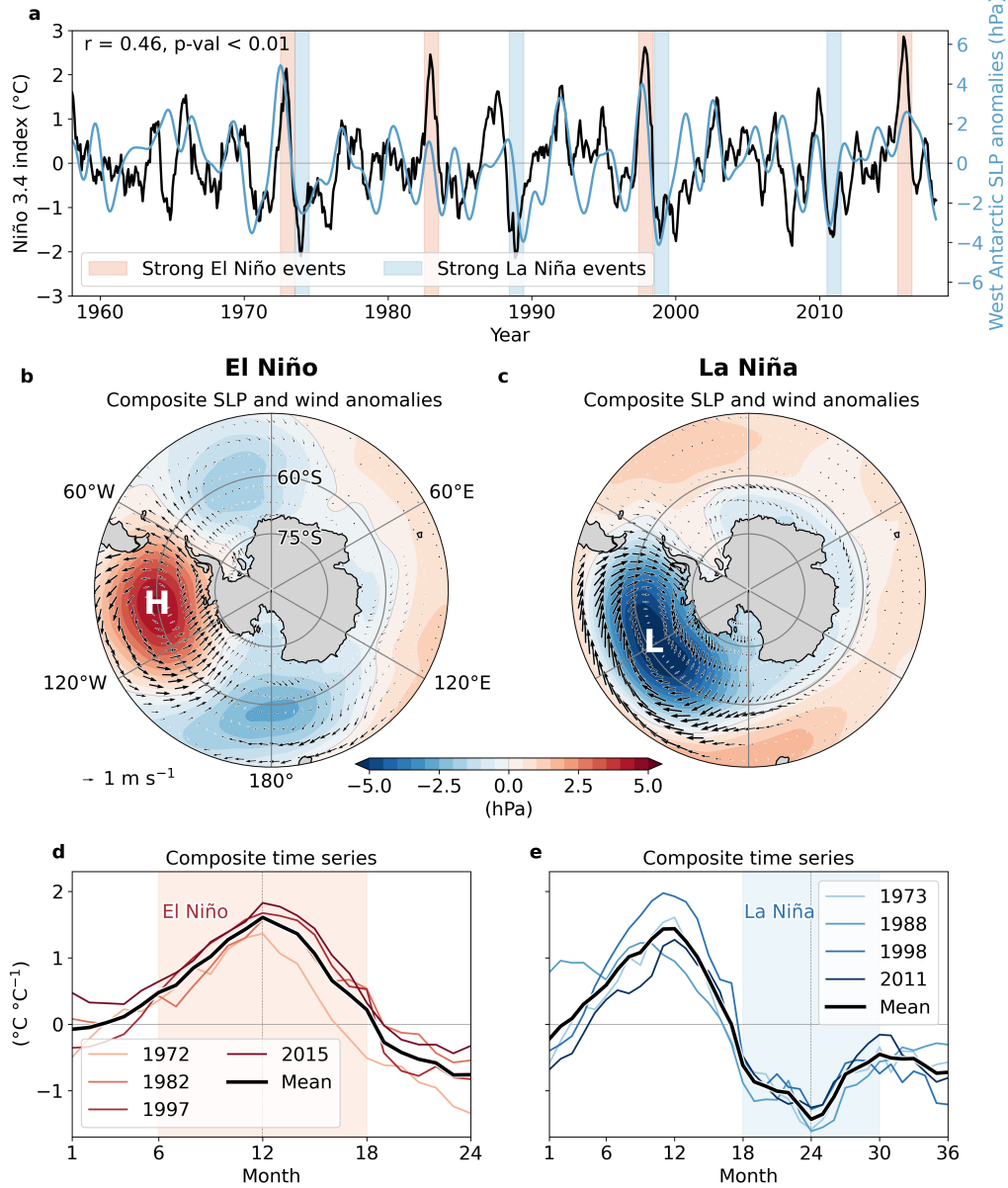


Figure 1. Time series and spatial patterns highlighting the teleconnection between ENSO and West Antarctica. (a) Time series of the Niño 3.4 index (the mean SST anomalies ($^{\circ}\text{C}$) in the region 5°S – 5°N and 170°W – 120°W) and mean West Antarctic sea level pressure (SLP) anomalies in the region 80°S – 45°S and 60°W – 150°W (hPa). The peak periods of four strong ENSO events are shaded in orange and blue respectively. A 3-pole low-pass filter at $1/10$ Nyquist frequency has been applied to the SLP time series. In the top left is the correlation coefficient (r) and significance value (p-val.) between the time series. (b, c) Composite mean SLP (hPa, colour shaded) and surface wind anomalies (m s^{-1} , arrows) during the events shaded in (a). The **H** and **L** symbols indicate the location of the largest SLP anomalies. (d, e) Composite time series based on the Niño 3.4 index during the events shaded in (a), centered at months 12 and 24 respectively. These time series are divided by the mean Niño 3.4 index during the four strongest events and unitless ($^{\circ}\text{C}/^{\circ}\text{C}$).

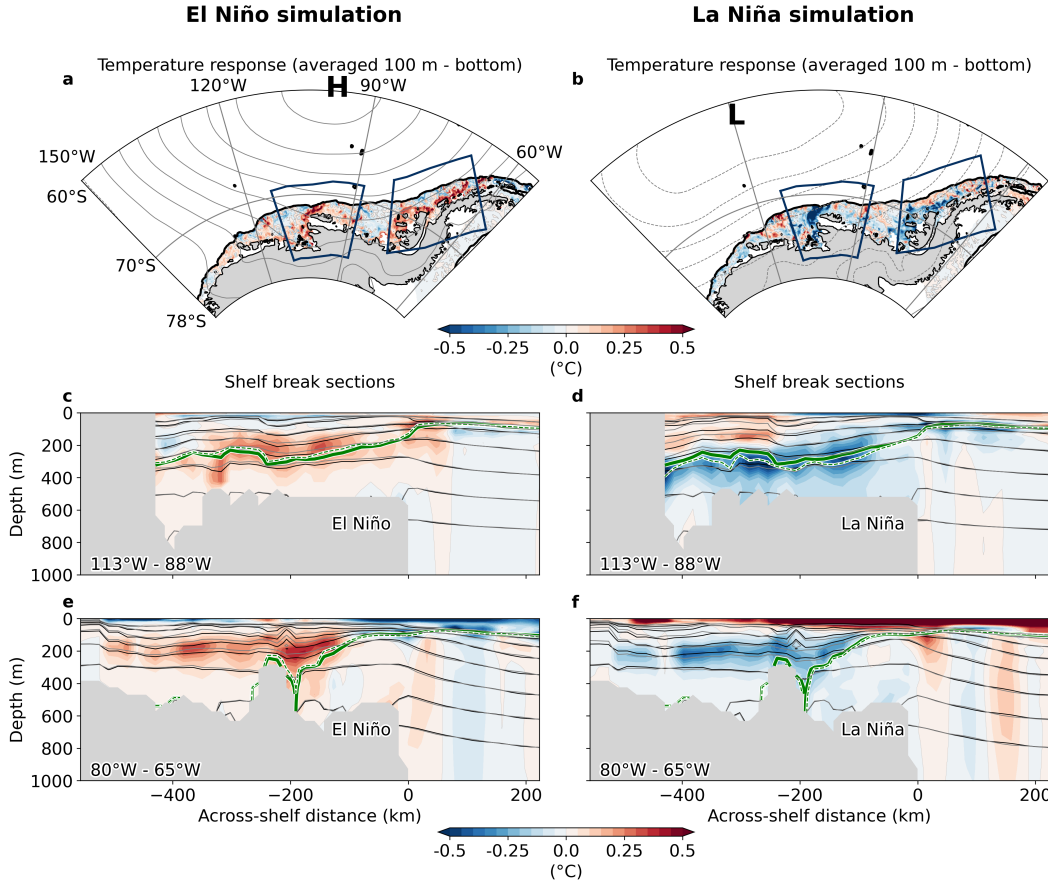


Figure 2. Response of the West Antarctic shelf during the peak of the El Niño and La Niña simulations. (a, b) Mean subsurface shelf temperature response ($^{\circ}\text{C}$). The 1000 m isobath is given as the black contour. The cross-shelf rectangles outline the regions for the depth-latitude panels in c-f. The grey contours show SLP anomalies (solid positive, dashed negative), with the **H** and **L** symbols indicating the location of the largest anomalies. (c-f) Mean cross-shelf temperature anomalies ($^{\circ}\text{C}$) in the regions outlined above, with the alongshore mean taken relative to the 1000 m isobath. These panels were created by subsetting the data into rectangles of along-shelf length of 72 km, each perpendicular to the 1000 m isobath at their centre point, and then taking the along-shelf average within and between each rectangle for each region. The bold and dashed green lines are the climatological and event 0°C isotherms. The 0°C isotherms near the surface region have been masked out. The black contours represent the climatological isopycnals and the grey contours the isopycnals during the events (potential density in 0.1 kg m^{-3} intervals between 1027.3 and 1028 kg m^{-3}).

References

- 324
Assmann, K. M., Jenkins, A., Shoosmith, D. R., Walker, D. P., Jacobs, S. S., & Nicholls,
325
K. W. (2013). Variability of Circumpolar Deep Water transport onto the Amundsen
326
Sea continental shelf through a shelf break trough. *Journal of Geophysical Research: Oceans*, 118(12), 6603-6620. doi: <https://doi.org/10.1002/2013JC008871>
327
Bett, D. T., Holland, P. R., Naveira Garabato, A. C., Jenkins, A., Dutrieux, P., Kimura, S.,
328
& Fleming, A. (2020). The impact of the Amundsen Sea freshwater balance on ocean
329
melting of the West Antarctic ice sheet. *Journal of Geophysical Research: Oceans*,
330
331

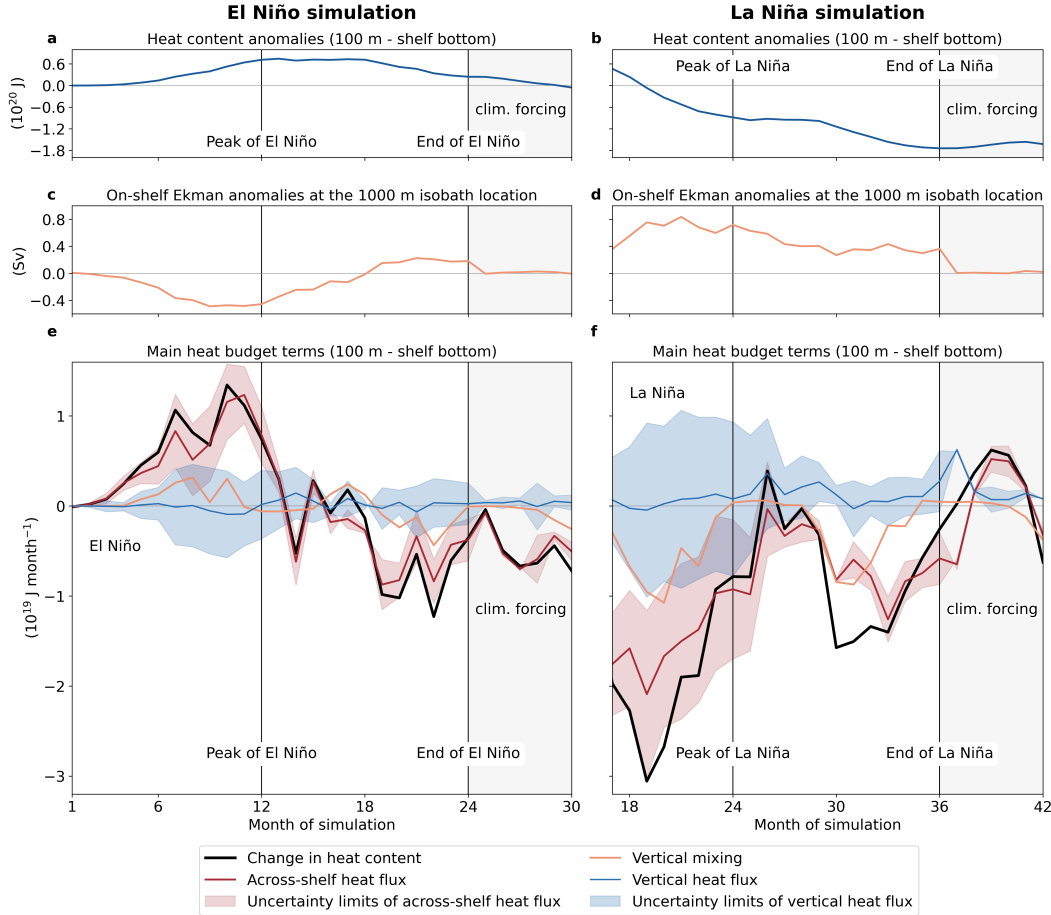


Figure 3. Time series of West Antarctic subsurface heat content anomalies, Ekman transport anomalies and the main heat budget terms during the El Niño and La Niña simulations. (a, b) The mean subsurface heat anomalies (10^{20} J) on the West Antarctic shelf (between 100 m, the shelf bottom, 150°W - 60°W and south of the 1000 m isobath location). The vertical lines indicate the peak and end of the simulated event. The grey shaded period indicates the six month extension of the simulation with climatological forcing. (c, d) The total on-shelf Ekman transport anomalies (Sv , $1 \text{ Sv} = 10^6 \text{ m}^3 \text{ s}^{-1}$) at the location of the 1000 m isobath. (e, f) The main Eulerian heat budget terms on the West Antarctic shelf (10^{19} J). The colour-shaded intervals indicate the uncertainties in the cross-shelf and vertical heat fluxes that represent the ambiguity of the return flow of heat re-entering the West Antarctic region (Section 3.2). Small, second-order terms are shown in Fig. S8.

332

125(9), e2020JC016305. doi: <https://doi.org/10.1029/2020JC016305>

333

Boehme, L., & Rosso, I. (2021). Classifying oceanographic structures in the Amundsen Sea, Antarctica. *Geophysical Research Letters*, 48(5), e2020GL089412. doi: <https://doi.org/10.1029/2020GL089412>

334

Cai, W., Borlace, S., Lengaigne, M., Van Renssch, P., Collins, M., Vecchi, G., ... others (2014). Increasing frequency of extreme El Niño events due to greenhouse warming. *Nature Climate Change*, 4(2), 111–116. doi: <https://doi.org/10.1038/nclimate2100>

335

Cai, W., Jia, F., Li, S., Purich, A., Wang, G., Wu, L., ... McPhaden, M. J. (2023). Antarctic shelf ocean warming and sea ice melt affected by projected El Niño changes. *Nature Climate Change*. doi: <https://doi.org/10.1038/s41558-023-01610-x>

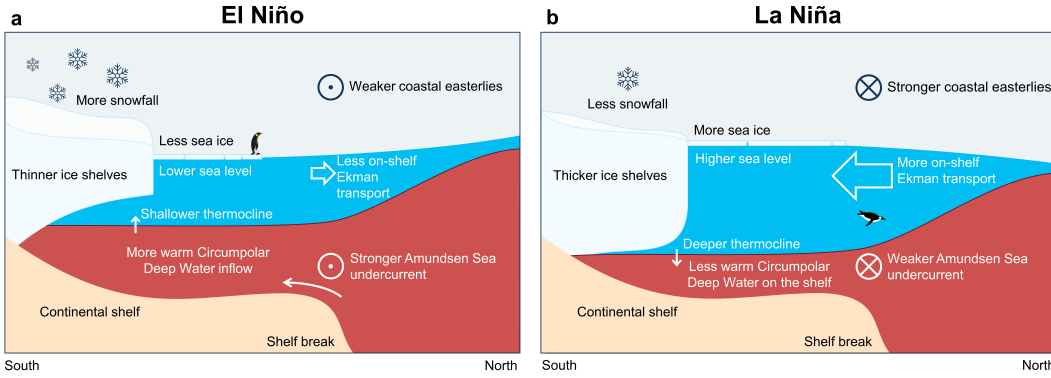


Figure 4. Simplified schematic of physical changes on the West Antarctic continental shelf during (a) El Niño and (b) La Niña events. During El Niño, the Amundsen Sea Low (ASL) and coastal easterlies weaken (Fig. 1b), they decrease on-shelf Ekman transport of cold surface water (Fig. 3c) and decrease sea level on the shelf (Fig. S16a). The symbols ⊖ and ⊕ show the anomalous anticyclonic (anticlockwise)/cyclonic ASL circulation and the large white arrows show the anomalous Ekman transport. The tilt in sea level then results in a barotropic pressure gradient and on-shelf heat transport via several possible mechanisms; 1) bottom Ekman transport, 2) baroclinic adjustment and shoaling of the isopycnals, 3) heat transport associated with strengthening of the eastward flowing Amundsen Sea undercurrent (the ⊖ symbol) and 4) eddy heat fluxes. El Niño also increases snowfall over West Antarctic ice shelves (Fig. S3g), decreases their mass (Paolo et al., 2018) and reduces sea ice volume (Fig. S9c). During La Niña, a largely opposite response occurs; the ASL and coastal easterlies strengthen (Fig. 1c), on-shelf Ekman transport and shelf sea level increase (Figs. 3d and S16b), in turn decreasing cross-shelf CDW transport via opposite mechanisms. La Niña also reduces snowfall (Fig. S4g), increases ice shelf mass (Paolo et al., 2018) and sea ice volume (Fig. S9d) compared to El Niño. The emperor penguins have been added as artistic expression. Ecological impacts on seabirds have not been investigated here.

- 342 Cai, W., Santoso, A., Collins, M., Dewitte, B., Karamperidou, C., Kug, J.-S., ... Zhong,
343 W. (2021). Changing El Niño–Southern Oscillation in a warming climate. *Nature
Reviews Earth & Environment*, 2(9), 628–644. doi: <https://doi.org/10.1038/s43017-021-00199-z>
- 344 Cai, W., Wang, G., Santoso, A., McPhaden, M. J., Wu, L., Jin, F.-F., ... others (2015).
345 Increased frequency of extreme La Niña events under greenhouse warming. *Nature
Climate Change*, 5(2), 132–137. doi: <https://doi.org/10.1038/nclimate2492>
- 346 Chiodi, A. M., & Harrison, D. E. (2015). Global seasonal precipitation anomalies robustly
347 associated with El Niño and La Niña events—an OLR perspective. *Journal of Climate*,
348 28(15), 6133 - 6159. doi: <https://doi.org/10.1175/JCLI-D-14-00387.1>
- 349 COSIMA. (2020). *COSIMA model output collection*. National Computational Facility.
350 ([Dataset]) doi: <https://doi.org/10.4225/41/5a2dc8543105a>
- 351 Davis, P. E. D., Nicholls, K. W., Holland, D. M., Schmidt, B. E., Washam, P., Riverman,
352 K. L., ... Makinson, K. (2023). Suppressed basal melting in the eastern Thwaites
353 Glacier grounding zone. *Nature*, 614(7948), 479–485. doi: <https://doi.org/10.1038/s41586-022-05586-0>
- 354 Dawson, H. R. S., Morrison, A. K., England, M. H., & Tamsitt, V. (2023). Pathways
355 and timescales of connectivity around the Antarctic continental shelf. *Journal of
356 Geophysical Research: Oceans*, 128(2), e2022JC018962. doi: <https://doi.org/10.1029/2022JC018962>
- 357 Depoorter, M. A., Bamber, J. L., Griggs, J. A., Lenaerts, J. T. M., Ligtenberg, S. R. M.,
358

- 363 van den Broeke, M. R., & Moholdt, G. (2013). Calving fluxes and basal melt rates
 364 of Antarctic ice shelves. *Nature*, 502(7469), 89–92. doi: <https://doi.org/10.1038/nature12567>
- 365 Dommeneget, D., Bayr, T., & Frauen, C. (2013). Analysis of the non-linearity in the pattern
 366 and time evolution of El Niño Southern Oscillation. *Climate Dynamics*, 40(11), 2825–
 367 2847. doi: <https://doi.org/10.1007/s00382-012-1475-0>
- 368 Dotto, T. S., Heywood, K. J., Hall, R. A., Scambos, T. A., Zheng, Y., Nakayama, Y.,
 369 ... Pettit, E. (2022). Ocean variability beneath Thwaites Eastern Ice Shelf driven
 370 by the Pine Island Bay Gyre strength. *Nature Communications*, 13(1), 7840. doi:
 371 10.1038/s41467-022-35499-5
- 372 Dutrieux, P., Rydt, J. D., Jenkins, A., Holland, P. R., Ha, H. K., Lee, S. H., ... Schröder,
 373 M. (2014). Strong sensitivity of pine island ice-shelf melting to climatic variability.
 374 *Science*, 343(6167), 174–178. doi: 10.1126/science.1244341
- 375 Fogt, R. L., & Bromwich, D. H. (2006). Decadal variability of the ENSO teleconnection to
 376 the high-latitude South Pacific governed by coupling with the Southern Annular Mode.
 377 *Journal of Climate*, 19(6), 979 - 997. doi: <https://doi.org/10.1175/JCLI3671.1>
- 378 Fogt, R. L., Bromwich, D. H., & Hines, K. M. (2011). Understanding the SAM influence on
 379 the South Pacific ENSO teleconnection. *Climate Dynamics*, 36(7), 1555–1576. doi:
 380 <https://doi.org/10.1007/s00382-010-0905-0>
- 381 Foppert, A., Rintoul, S. R., Purkey, S. G., Zilberman, N., Kobayashi, T., Sallée, J.-B., ...
 382 Wallace, L. O. (2021). Deep Argo reveals bottom water properties and pathways in
 383 the Australian-Antarctic basin. *Journal of Geophysical Research: Oceans*, 126(12),
 384 e2021JC017935. doi: <https://doi.org/10.1029/2021JC017935>
- 385 Forget, G., & Ferreira, D. (2019). Global ocean heat transport dominated by heat export
 386 from the tropical Pacific. *Nature Geoscience*, 12(5), 351–354. doi: <https://doi.org/10.1038/s41561-019-0333-7>
- 387 Friedrichs, D. M., McInerney, J. B. T., Oldroyd, H. J., Lee, W. S., Yun, S., Yoon, S.-T.,
 388 ... Forrest, A. L. (2022). Observations of submesoscale eddy-driven heat transport
 389 at an ice shelf calving front. *Communications Earth & Environment*, 3(1), 140. doi:
 390 <https://doi.org/10.1038/s43247-022-00460-3>
- 391 Fürst, J. J., Durand, G., Gillet-Chaulet, F., Tavard, L., Rankl, M., Braun, M., & Gagliardi,
 392 O. (2016). The safety band of Antarctic ice shelves. *Nature Climate Change*,
 393 6(5), 479–482. doi: <https://doi.org/10.1038/nclimate2912>
- 394 Goyal, R., Jucker, M., Gupta, A. S., & England, M. H. (2022). A new zonal wave-3
 395 index for the Southern Hemisphere. *Journal of Climate*, 35(15), 5137 - 5149. doi:
 396 <https://doi.org/10.1175/JCLI-D-21-0927.1>
- 397 Goyal, R., Jucker, M., Sen Gupta, A., Hendon, H. H., & England, M. H. (2021). Zonal
 398 wave 3 pattern in the Southern Hemisphere generated by tropical convection. *Nature
 399 Geoscience*, 14(10), 732–738. doi: <https://doi.org/10.1038/s41561-021-00811-3>
- 400 Goyal, R., Sen Gupta, A., Jucker, M., & England, M. H. (2021). Historical and projected
 401 changes in the Southern Hemisphere surface westerlies. *Geophysical Research Letters*,
 402 48(4), e2020GL090849. doi: <https://doi.org/10.1029/2020GL090849>
- 403 Greene, C. A., Gardner, A. S., Schlegel, N.-J., & Fraser, A. D. (2022). Antarctic calving loss
 404 rivals ice-shelf thinning. *Nature*. doi: <https://doi.org/10.1038/s41586-022-05037-w>
- 405 Griffies, S. M. (2012). Elements of the modular ocean model (MOM). *GFDL Ocean Group
 406 Tech. Rep.*, 7, 620.
- 407 Gudmundsson, G. H. (2013). Ice-shelf buttressing and the stability of marine ice sheets.
 408 *The Cryosphere*, 7(2), 647–655. doi: <https://doi.org/10.5194/tc-7-647-2013>
- 409 Gudmundsson, G. H., Paolo, F. S., Adusumilli, S., & Fricker, H. A. (2019). Instantaneous
 410 Antarctic ice sheet mass loss driven by thinning ice shelves. *Geophysical Research
 411 Letters*, 46(23), 13903-13909. doi: <https://doi.org/10.1029/2019GL085027>
- 412 Heuzé, C. (2021). Antarctic Bottom Water and North Atlantic Deep Water in CMIP6
 413 models. *Ocean Science*, 17(1), 59–90. doi: <https://doi.org/10.5194/os-17-59-2021>
- 414 Heuzé, C., Heywood, K. J., Stevens, D. P., & Ridley, J. K. (2013). Southern Ocean bottom
 415 water characteristics in CMIP5 models. *Geophysical Research Letters*, 40(7), 1409–
- 416

- 418 1414. doi: <https://doi.org/10.1002/grl.50287>
- 419 Heywood, K. J., Biddle, L. C., Boehme, L., Dutrieux, P., Fedak, M., Jenkins, A., ...
 420 Webber, B. G. (2016, December). Between the Devil and the deep blue sea: the role
 421 of the Amundsen Sea continental shelf in exchanges between ocean and ice shelves.
 422 *Oceanography*. doi: <https://doi.org/10.5670/oceanog.2016.104>
- 423 Holmes, R. M., Zika, J. D., Ferrari, R., Thompson, A. F., Newsom, E. R., & England,
 424 M. H. (2019). Atlantic ocean heat transport enabled by Indo-Pacific heat uptake
 425 and mixing. *Geophysical Research Letters*, *46*(23), 13939-13949. doi: <https://doi.org/10.1029/2019GL085160>
- 427 Hoskins, B. J., & Ambrizzi, T. (1993). Rossby wave propagation on a realistic longitudinally
 428 varying flow. *Journal of Atmospheric Sciences*, *50*(12), 1661 - 1671. doi: [https://doi.org/10.1175/1520-0469\(1993\)050<1661:RWPOAR>2.0.CO;2](https://doi.org/10.1175/1520-0469(1993)050<1661:RWPOAR>2.0.CO;2)
- 430 Huguenin, M. F. (2023a). *ENSO-Antarctica_data* (Version 20231027_1306). Zenodo.
 431 ([Dataset]) doi: <https://doi.org/10.5281/zenodo.10045880>
- 432 Huguenin, M. F. (2023b). *ENSO-Antarctica_scripts* (Version 20231027). Zenodo. ([Soft-
 433 ware]) doi: <https://doi.org/10.5281/zenodo.8041423>
- 434 Huguenin, M. F., Holmes, R. M., & England, M. H. (2022). Drivers and distribution of
 435 global ocean heat uptake over the last half century. *Nature Communications*, *13*(1),
 436 4921. doi: <https://doi.org/10.1038/s41467-022-32540-5>
- 437 Huneke, W. G. C., Morrison, A. K., & Hogg, A. M. (2022). Spatial and subannual variability
 438 of the Antarctic Slope Current in an eddying ocean-sea ice model. *Journal of Physical
 439 Oceanography*, *52*(3), 347 - 361. doi: <https://doi.org/10.1175/JPO-D-21-0143.1>
- 440 Hunke, E., Lipscomb, W., & Turner, A. (2015). CICE: the Los Alamos sea ice model,
 441 documentation and software, version 5.1 (Tech. Rep. LA-CC-06-012). *Los Alamos
 442 National Laboratory*.
- 443 Jacobs, S., & Huber, B. (2016). *Processed temperature, salinity, and current measure-
 444 ment data from the Amundsen Sea acquired during the Nathaniel B. Palmer expedi-
 445 tion NBP0901 (2009)*. Interdisciplinary Earth Data Alliance (IEDA). ([Dataset]) doi:
 446 <https://doi.org/10.1594/IEDA/322014>
- 447 Jacobs, S. S., Jenkins, A., Giulivi, C. F., & Dutrieux, P. (2011). Stronger ocean circulation
 448 and increased melting under Pine Island Glacier ice shelf. *Nature Geoscience*, *4*(8),
 449 519–523. doi: <https://doi.org/10.1038/ngeo1188>
- 450 Jenkins, A., Dutrieux, P., Jacobs, S., Steig, E. J., Gudmundsson, G. H., Smith, J., &
 451 Heywood, K. J. (2016). Decadal ocean forcing and Antarctic ice sheet response:
 452 lessons from the Amundsen Sea. *Oceanography*.
- 453 Jenkins, A., Shoosmith, D., Dutrieux, P., Jacobs, S., Kim, T. W., Lee, S. H., ...
 454 Stammerjohn, S. (2018). West Antarctic Ice Sheet retreat in the Amundsen Sea
 455 driven by decadal oceanic variability. *Nature Geoscience*, *11*(10), 733–738. doi:
 456 <https://doi.org/10.1038/s41561-018-0207-4>
- 457 Karoly, D. J. (1989). Southern Hemisphere circulation features associated with El Niño-
 458 Southern Oscillation events. *Journal of Climate*, *2*(11), 1239 - 1252. doi: [https://doi.org/10.1175/1520-0442\(1989\)002<1239:SHCFAW>2.0.CO;2](https://doi.org/10.1175/1520-0442(1989)002<1239:SHCFAW>2.0.CO;2)
- 460 Keppler, L., & Landschützer, P. (2019). Regional wind variability modulates the Southern
 461 Ocean carbon sink. *Scientific Reports*, *9*(1), 7384. doi: <https://doi.org/10.1038/s41598-019-43826-y>
- 463 Kim, T.-W., Yang, H. W., Dutrieux, P., Wåhlin, A. K., Jenkins, A., Kim, Y. G., ...
 464 Cho, Y.-K. (2021). Interannual variation of modified Circumpolar Deep Water in
 465 the Dotson-Getz Trough, West Antarctica. *Journal of Geophysical Research: Oceans*,
 466 *126*(12), e2021JC017491. doi: <https://doi.org/10.1029/2021JC017491>
- 467 Kimura, S., Jenkins, A., Regan, H., Holland, P. R., Assmann, K. M., Whitt, D. B., ...
 468 Dutrieux, P. (2017). Oceanographic controls on the variability of ice-shelf basal melting
 469 and circulation of glacial meltwater in the Amundsen Sea Embayment, Antarctica.
 470 *Journal of Geophysical Research: Oceans*, *122*(12), 10131-10155. doi: <https://doi.org/10.1002/2017JC012926>
- 472 Kiss, A. E., Hogg, A. M., Hannah, N., Boeira Dias, F., Brassington, G. B., Chamberlain,

- M. A., ... Zhang, X. (2020). ACCESS-OM2: a global ocean-sea ice model at three resolutions. *Geoscientific Model Development Discussions*, 1–58. doi: <https://doi.org/10.5194/gmd-13-401-2020>
- Lachlan-Cope, T., & Connolley, W. (2006). Teleconnections between the tropical Pacific and the Amundsen-Bellinghausen Sea: role of the El Niño/Southern Oscillation. *Journal of Geophysical Research: Atmospheres*, 111(D23). doi: <https://doi.org/10.1029/2005JD006386>
- Li, Q., England, M. H., Hogg, A. M., Rintoul, S. R., & Morrison, A. K. (2023). Abyssal ocean overturning slowdown and warming driven by Antarctic meltwater. *Nature*, 615(7954), 841–847. doi: <https://doi.org/10.1038/s41586-023-05762-w>
- Locarnini, R. A., Mishonov, A. V., Antonov, J. I., Boyer, T. P., Garcia, H. E., Baranova, O. K., ... others (2013). World Ocean Atlas 2013, volume 1: temperature. In L. S (Ed.), *NOAA Atlas NESDIS 73:40* (p. 40 pp). US Government Printing Office, Washington D.C.
- Marshall, G. J. (2003). Trends in the Southern Annular Mode from observations and reanalyses. *Journal of Climate*, 16(24), 4134 - 4143. doi: [https://doi.org/10.1175/1520-0442\(2003\)016<4134:TITSAM>2.0.CO;2](https://doi.org/10.1175/1520-0442(2003)016<4134:TITSAM>2.0.CO;2)
- Martinson, D. G., Stammerjohn, S. E., Iannuzzi, R. A., Smith, R. C., & Vernet, M. (2008). Western Antarctic Peninsula physical oceanography and spatio-temporal variability. *Deep Sea Research Part II: Topical Studies in Oceanography*, 55(18), 1964–1987. doi: <https://doi.org/10.1016/j.dsr2.2008.04.038>
- Mazloff, M. R., Heimbach, P., & Wunsch, C. (2010). An eddy-permitting Southern Ocean state estimate. *Journal of Physical Oceanography*, 40(5), 880 - 899. doi: <https://doi.org/10.1175/2009JPO4236.1>
- McGregor, S., Cassou, C., Kosaka, Y., & Phillips, A. S. (2022). Projected ENSO teleconnection changes in CMIP6. *Geophysical Research Letters*, 49(11), e2021GL097511. doi: <https://doi.org/10.1029/2021GL097511>
- Moorman, R., Thompson, A. F., & Wilson, E. A. (2023). Coastal polynyas enable transitions between high and low West Antarctic ice shelf melt rates. *Geophysical Research Letters*, 50(16), e2023GL104724. doi: <https://doi.org/10.1029/2023GL104724>
- Nakayama, Y., Schröder, M., & Hellmer, H. (2013). From Circumpolar Deep Water to the glacial meltwater plume on the eastern Amundsen Shelf. *Deep Sea Research Part I: Oceanographic Research Papers*, 77, 50-62. doi: <https://doi.org/10.1016/j.dsr.2013.04.001>
- Naughten, K. A., Holland, P. R., & De Rydt, J. (2023). Unavoidable future increase in West Antarctic ice-shelf melting over the twenty-first century. *Nature Climate Change*. doi: <https://doi.org/10.1038/s41558-023-01818-x>
- Naughten, K. A., Holland, P. R., Dutrieux, P., Kimura, S., Bett, D. T., & Jenkins, A. (2022). Simulated twentieth-century ocean warming in the Amundsen Sea, West Antarctica. *Geophysical Research Letters*, 49(5), e2021GL094566. doi: <https://doi.org/10.1029/2021GL094566>
- Oelerich, R., Heywood, K. J., Damerell, G. M., & Thompson, A. F. (2022). Wind-induced variability of warm water on the southern Bellingshausen Sea continental shelf. *Journal of Geophysical Research: Oceans*, 127(11), e2022JC018636. doi: <https://doi.org/10.1029/2022JC018636>
- Okumura, Y. M., & Deser, C. (2010). Asymmetry in the duration of El Niño and La Niña. *Journal of Climate*, 23(21), 5826–5843. doi: <https://doi.org/10.1175/2010JCLI3592.1>
- Paolo, F. S., Fricker, H. A., & Padman, L. (2015). Volume loss from Antarctic ice shelves is accelerating. *Science*, 348(6232), 327-331. doi: <https://doi.org/10.1126/science.aaa0940>
- Paolo, F. S., Padman, L., Fricker, H. A., Adusumilli, S., Howard, S., & Siegfried, M. R. (2018). Response of Pacific-sector Antarctic ice shelves to the El Niño/Southern Oscillation. *Nature Geoscience*, 11, 121-126. doi: <https://doi.org/10.1038/s41561-017-0033-0>

- 528 Pritchard, H. D., Ligtenberg, S. R. M., Fricker, H. A., Vaughan, D. G., van den Broeke,
 529 M. R., & Padman, L. (2012). Antarctic ice-sheet loss driven by basal melting of ice
 530 shelves. *Nature*, *484*(7395), 502–505. doi: <https://doi.org/10.1038/nature10968>
- 531 Purich, A., & England, M. H. (2021). Historical and future projected warming of Antarc-
 532 tic Shelf Bottom Water in CMIP6 models. *Geophysical Research Letters*, *48*(10),
 533 e2021GL092752. doi: <https://doi.org/10.1029/2021GL092752>
- 534 Raphael, M. N., Marshall, G. J., Turner, J., Fogt, R. L., Schneider, D., Dixon, D. A., ...
 535 Hobbs, W. R. (2016). The Amundsen Sea Low: variability, change, and impact on
 536 Antarctic climate. *Bulletin of the American Meteorological Society*, *97*(1), 111 - 121.
 537 doi: <https://doi.org/10.1175/BAMS-D-14-00018.1>
- 538 Rignot, E., Mouginot, J., Scheuchl, B., van den Broeke, M., van Wessem, M. J., &
 539 Morlighem, M. (2019). Four decades of Antarctic Ice Sheet mass balance from
 540 1979–2017. *Proceedings of the National Academy of Sciences*, *116*(4), 1095-1103. doi:
 541 <https://doi.org/10.1073/pnas.1812883116>
- 542 Roquet, F., Wunsch, C., Forget, G., Heimbach, P., Guinet, C., Reverdin, G., ... Fedak,
 543 M. A. (2013). Estimates of the Southern Ocean general circulation improved by
 544 animal-borne instruments. *Geophysical Research Letters*, *40*(23), 6176-6180. doi:
 545 <https://doi.org/10.1002/2013GL058304>
- 546 Scambos, T., Bell, R., Alley, R., Anandakrishnan, S., Bromwich, D., Brunt, K., ... Yager,
 547 P. (2017). How much, how fast?: A science review and outlook for research on the
 548 instability of Antarctica's Thwaites Glacier in the 21st century. *Global and Planetary
 549 Change*, *153*, 16-34. doi: <https://doi.org/10.1016/j.gloplacha.2017.04.008>
- 550 Schmidtko, S., Heywood, K. J., Thompson, A. F., & Aoki, S. (2014). Multidecadal warming
 551 of Antarctic waters. *Science*, *346*(6214), 1227-1231. doi: <https://doi.org/10.1126/science.1256117>
- 553 Shepherd, A., Ivins, E., Rignot, E., Smith, B., van den Broeke, M., Velicogna, I., ... Team,
 554 T. I. (2018). Mass balance of the Antarctic Ice Sheet from 1992 to 2017. *Nature*,
 555 *558*(7709), 219–222. doi: <https://doi.org/10.1038/s41586-018-0179-y>
- 556 Silvano, A., Holland, P. R., Naughten, K. A., Dragomir, O., Dutrieux, P., Jenkins, A., ...
 557 Naveira Garabato, A. C. (2022). Baroclinic Ocean Response to Climate Forcing Reg-
 558 ulates Decadal Variability of Ice-Shelf Melting in the Amundsen Sea. *Geophysical Re-
 559 search Letters*, *49*(24), e2022GL100646. doi: <https://doi.org/10.1029/2022GL100646>
- 560 Spence, P., Griffies, S. M., England, M. H., Hogg, A. M., Saenko, O. A., & Jourdain, N. C.
 561 (2014). Rapid subsurface warming and circulation changes of Antarctic coastal waters
 562 by poleward shifting winds. *Geophysical Research Letters*, *41*(13), 4601-4610. doi:
 563 <https://doi.org/10.1002/2014GL060613>
- 564 Spence, P., Holmes, R. M., Hogg, A. M., Griffies, S. M., Stewart, K. D., & England, M. H.
 565 (2017). Localized rapid warming of West Antarctic subsurface waters by remote winds.
 566 *Nature Climate Change*, *7*(8), 595. doi: <https://doi.org/10.1038/nclimate3335>
- 567 Steig, E., Ding, Q., Battisti, D., & Jenkins, A. (2012). Tropical forcing of Circumpolar
 568 Deep Water inflow and outlet glacier thinning in the Amundsen Sea Embayment, West
 569 Antarctica. *Annals of Glaciology*, *53*(60), 19–28. doi: [10.3189/2012AoG60A110](https://doi.org/10.3189/2012AoG60A110)
- 570 Stewart, A. L., & Thompson, A. F. (2015). Eddy-mediated transport of warm Circumpolar
 571 Deep Water across the Antarctic Shelf Break. *Geophysical Research Letters*, *42*(2),
 572 432-440. doi: <https://doi.org/10.1002/2014GL062281>
- 573 Stewart, K., Kim, W., Urakawa, S., Hogg, A., Yeager, S., Tsujino, H., ... Danabasoglu, G.
 574 (2020). JRA55-do-based repeat year forcing datasets for driving ocean–sea-ice models.
 575 *Ocean Modelling*, *147*, 101557. doi: <https://doi.org/10.1016/j.ocemod.2019.101557>
- 576 St-Laurent, P., Klinck, J. M., & Dinniman, M. S. (2013). On the role of coastal troughs in the
 577 circulation of warm Circumpolar Deep Water on Antarctic shelves. *Journal of Physical
 578 Oceanography*, *43*(1), 51 - 64. doi: <https://doi.org/10.1175/JPO-D-11-0237.1>
- 579 St-Laurent, P., Klinck, J. M., & Dinniman, M. S. (2015). Impact of local winter cooling on
 580 the melt of pine island glacier, antarctica. *Journal of Geophysical Research: Oceans*,
 581 *120*(10), 6718-6732. doi: <https://doi.org/10.1002/2015JC010709>
- 582 Tamsitt, V., England, M. H., Rintoul, S. R., & Morrison, A. K. (2021). Residence time and

- transformation of warm circumpolar deep water on the Antarctic continental shelf. *Geophysical Research Letters*, 48(20). doi: <https://doi.org/10.1029/2021GL096092>
- Thoma, M., Jenkins, A., Holland, D., & Jacobs, S. (2008). Modelling circumpolar deep water intrusions on the amundsen sea continental shelf, antarctica. *Geophysical Research Letters*, 35(18). doi: <https://doi.org/10.1029/2008GL034939>
- Treasure, A., Roquet, F., Ansorge, I., Bester, M., Boehme, L., Bornemann, H., ... de Bruyn, P. (2017). Marine mammals exploring the oceans pole to pole: a review of the MEOP consortium. *Oceanography*.
- Tsujino, H., Urakawa, L. S., Griffies, S. M., Danabasoglu, G., Adcroft, A. J., Amaral, A. E., ... Yu, Z. (2020). Evaluation of global ocean–sea-ice model simulations based on the experimental protocols of the Ocean Model Intercomparison Project phase 2 (OMIP-2). *Geoscientific Model Development*, 13(8), 3643–3708. doi: <https://doi.org/10.5194/gmd-13-3643-2020>
- Tsujino, H., Urakawa, S., Nakano, H., Small, R. J., Kim, W. M., Yeager, S. G., ... others (2018). JRA-55 based surface dataset for driving ocean–sea-ice models (JRA55-do). *Ocean Modelling*, 130, 79–139. doi: <https://doi.org/10.1016/j.ocemod.2018.07.002>
- Turner, J. (2004). The El Niño–Southern Oscillation and Antarctica. *International Journal of Climatology*, 24(1), 1–31. doi: <https://doi.org/10.1002/joc.965>
- Vera, C. S., & Osman, M. (2018). Activity of the Southern Annular Mode during 2015–2016 El Niño event and its impact on Southern Hemisphere climate anomalies. *International Journal of Climatology*, 38(S1), e1288–e1295. doi: <https://doi.org/10.1002/joc.5419>
- Walker, C., & Gardner, A. (2017). Rapid drawdown of Antarctica’s Wordie Ice Shelf glaciers in response to ENSO/Southern Annular Mode-driven warming in the Southern Ocean. *Earth and Planetary Science Letters*, 476, 100–110. doi: <https://doi.org/10.1016/j.epsl.2017.08.005>
- Walker, D. P., Jenkins, A., Assmann, K. M., Shoosmith, D. R., & Brandon, M. A. (2013). Oceanographic observations at the shelf break of the Amundsen Sea, Antarctica. *Journal of Geophysical Research: Oceans*, 118(6), 2906–2918. doi: <https://doi.org/10.1002/jgrc.20212>
- Wang, G., Cai, W., Santoso, A., Wu, L., Fyfe, J. C., Yeh, S.-W., ... McPhaden, M. J. (2022). Future Southern Ocean warming linked to projected ENSO variability. *Nature Climate Change*, 12(7), 649–654. doi: <https://doi.org/10.1038/s41558-022-01398-2>
- Webb, D. J., Holmes, R. M., Spence, P., & England, M. H. (2022). Propagation of barotropic Kelvin waves around Antarctica. *Ocean Dynamics*, 72(6), 405–419. doi: [10.1007/s10236-022-01506-y](https://doi.org/10.1007/s10236-022-01506-y)
- Webber, B. G. M., Heywood, K. J., Stevens, D. P., Dutrieux, P., Abrahamsen, E. P., Jenkins, A., ... Kim, T. W. (2017). Mechanisms driving variability in the ocean forcing of Pine Island Glacier. *Nature Communications*, 8(1), 14507. doi: <https://doi.org/10.1038/ncomms14507>
- Wählin, A. K., Kalén, O., Arneborg, L., Björk, G., Carvajal, G. K., Ha, H. K., ... Stranne, C. (2013). Variability of warm deep water inflow in a submarine trough on the Amundsen Sea shelf. *Journal of Physical Oceanography*, 43(10), 2054 – 2070. doi: <https://doi.org/10.1175/JPO-D-12-0157.1>
- Wählin, A. K., Muench, R. D., Arneborg, L., Björk, G., Ha, H. K., Lee, S. H., & Alsén, H. (2012). Some implications of Ekman layer dynamics for cross-shelf exchange in the Amundsen Sea. *Journal of Physical Oceanography*, 42(9), 1461 – 1474. doi: <https://doi.org/10.1175/JPO-D-11-041.1>
- Zuo, H., Balmaseda, M. A., Tietsche, S., Mogensen, K., & Mayer, M. (2019). The ECMWF operational ensemble reanalysis–analysis system for ocean and sea ice: a description of the system and assessment. *Ocean Science*, 15(3), 779–808. doi: <https://doi.org/10.5194/os-15-779-2019>

Figure 1.

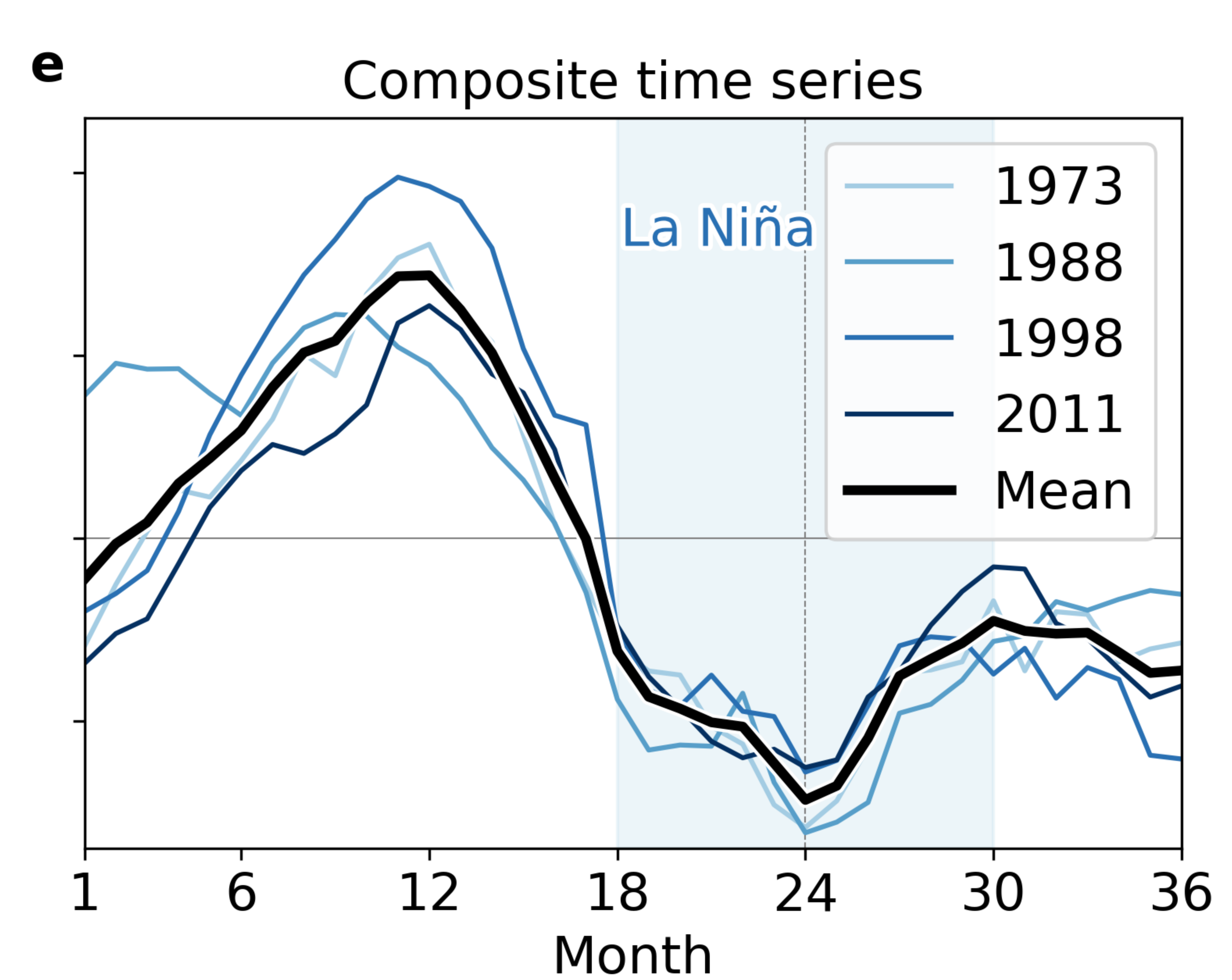
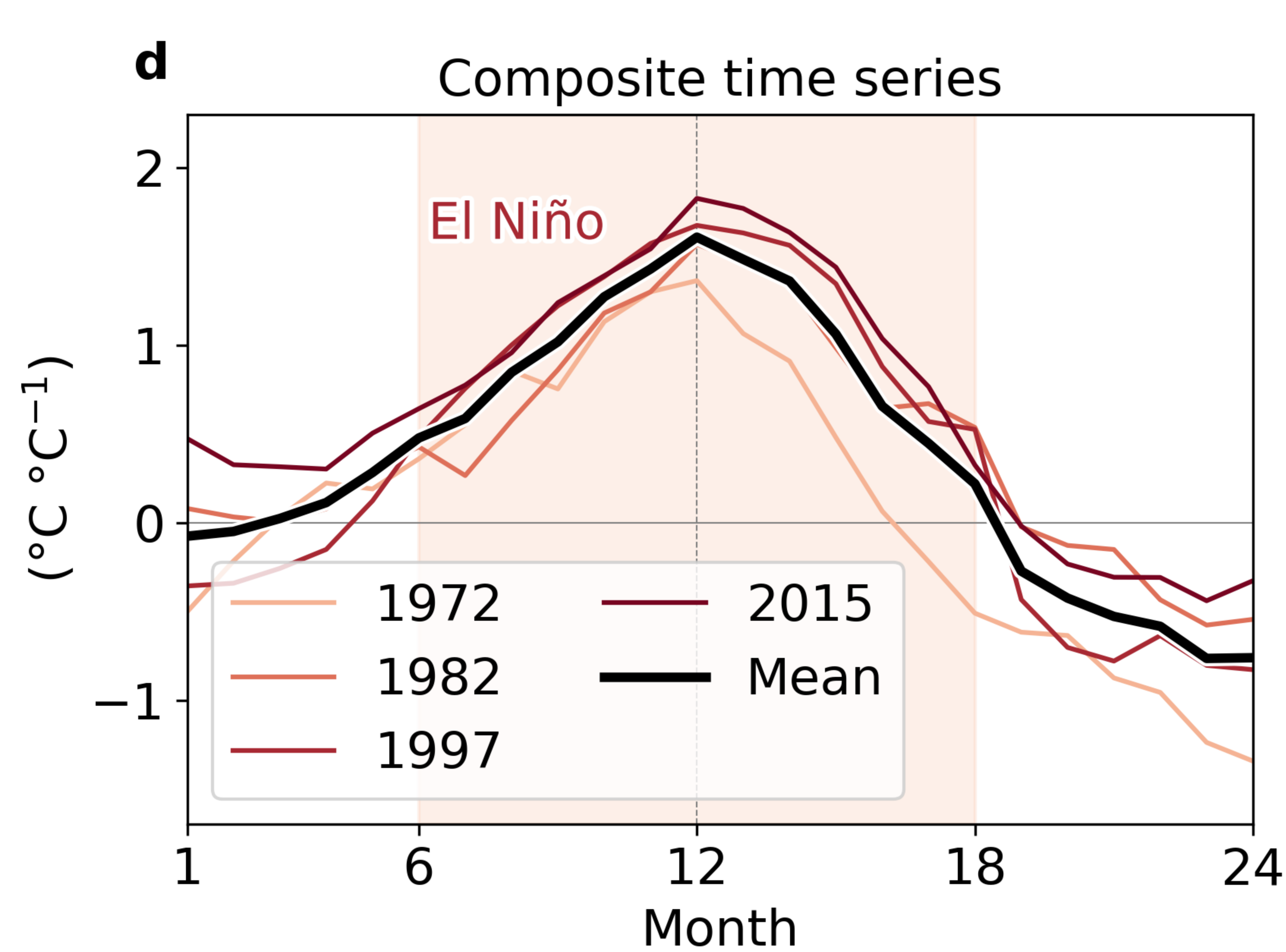
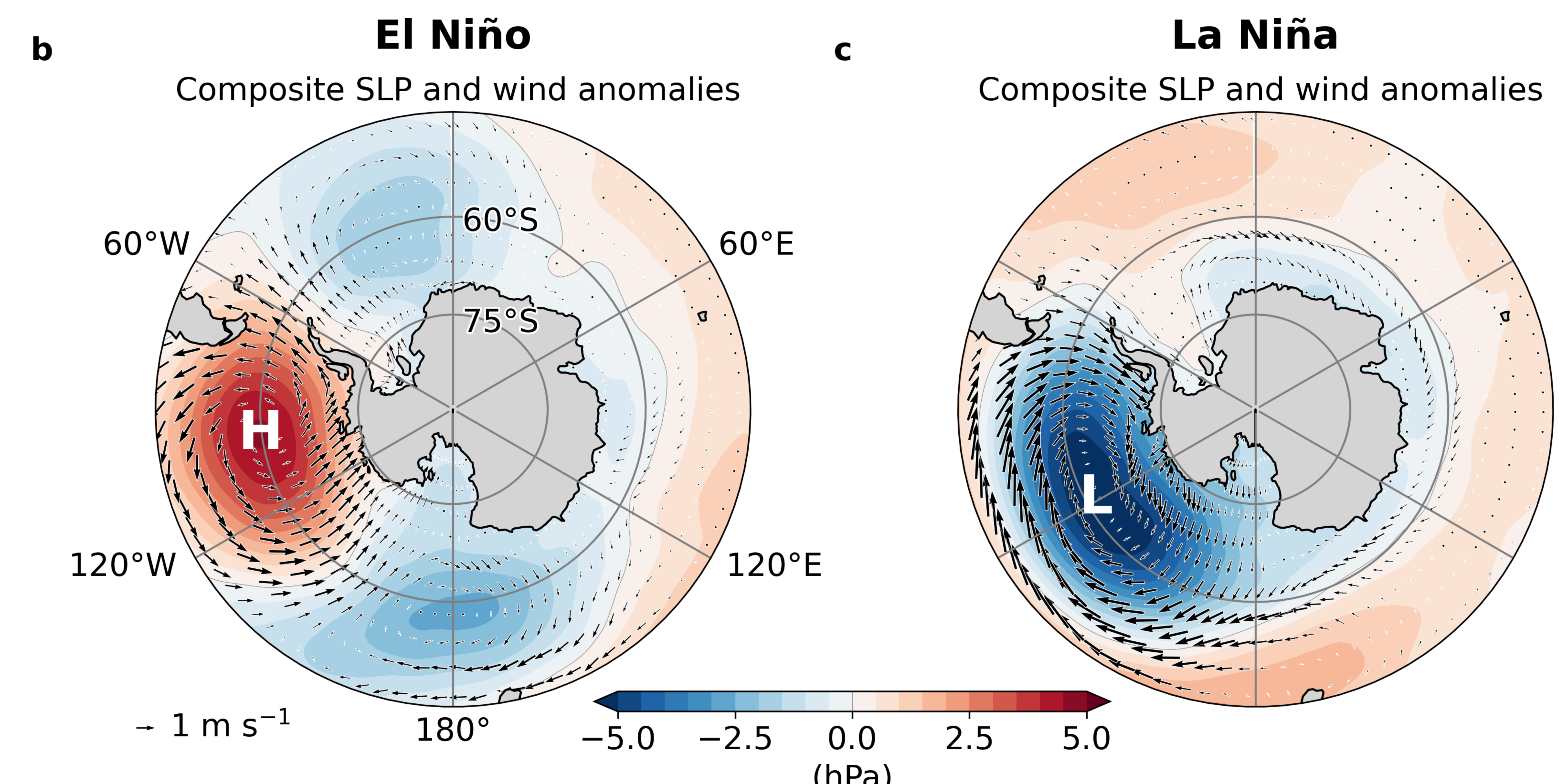
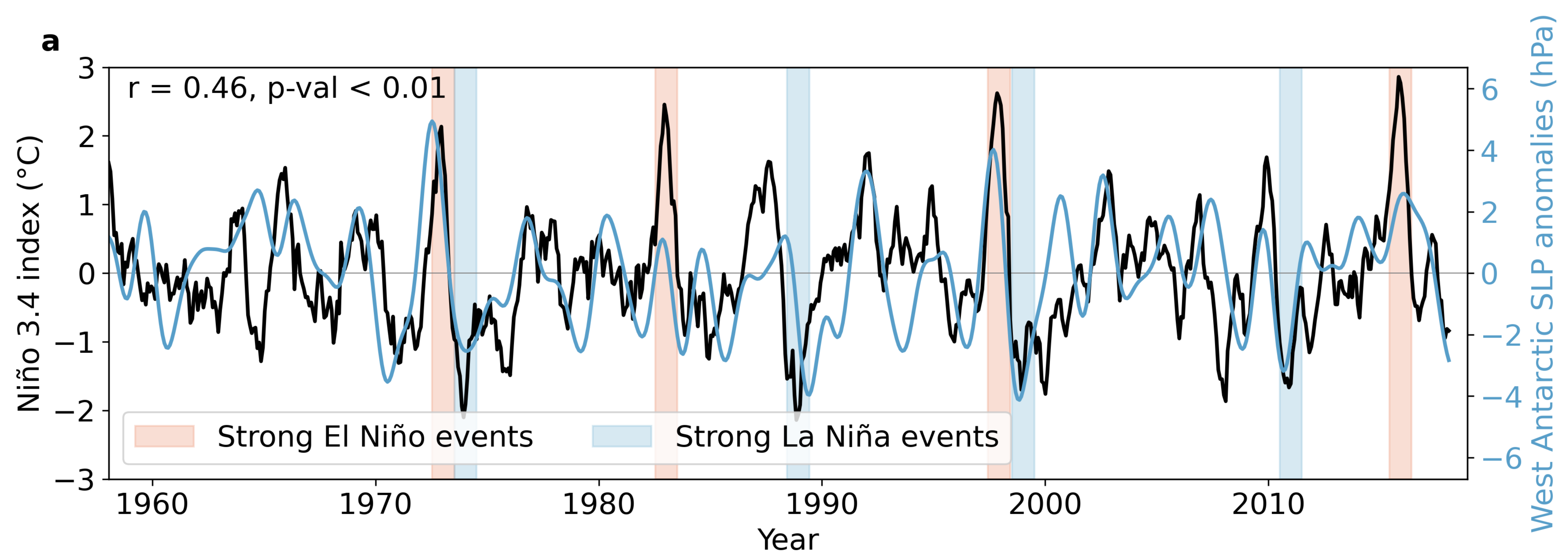


Figure 2.

El Niño simulation

La Niña simulation

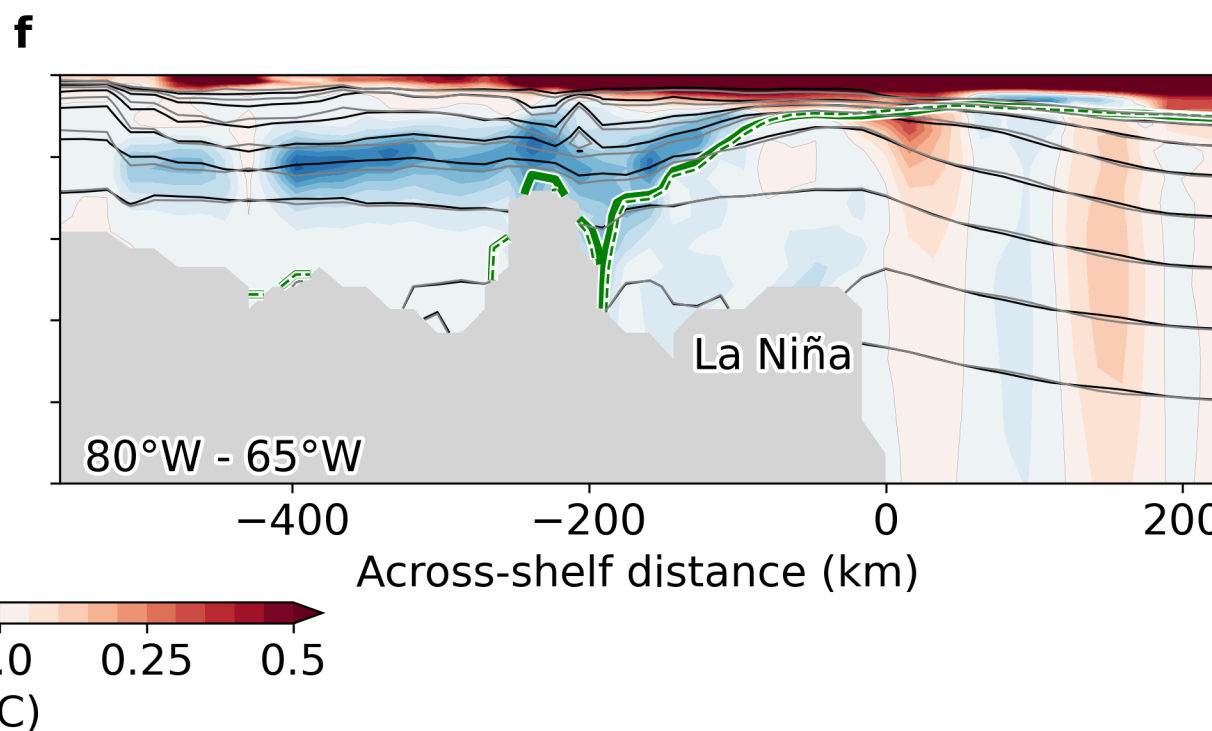
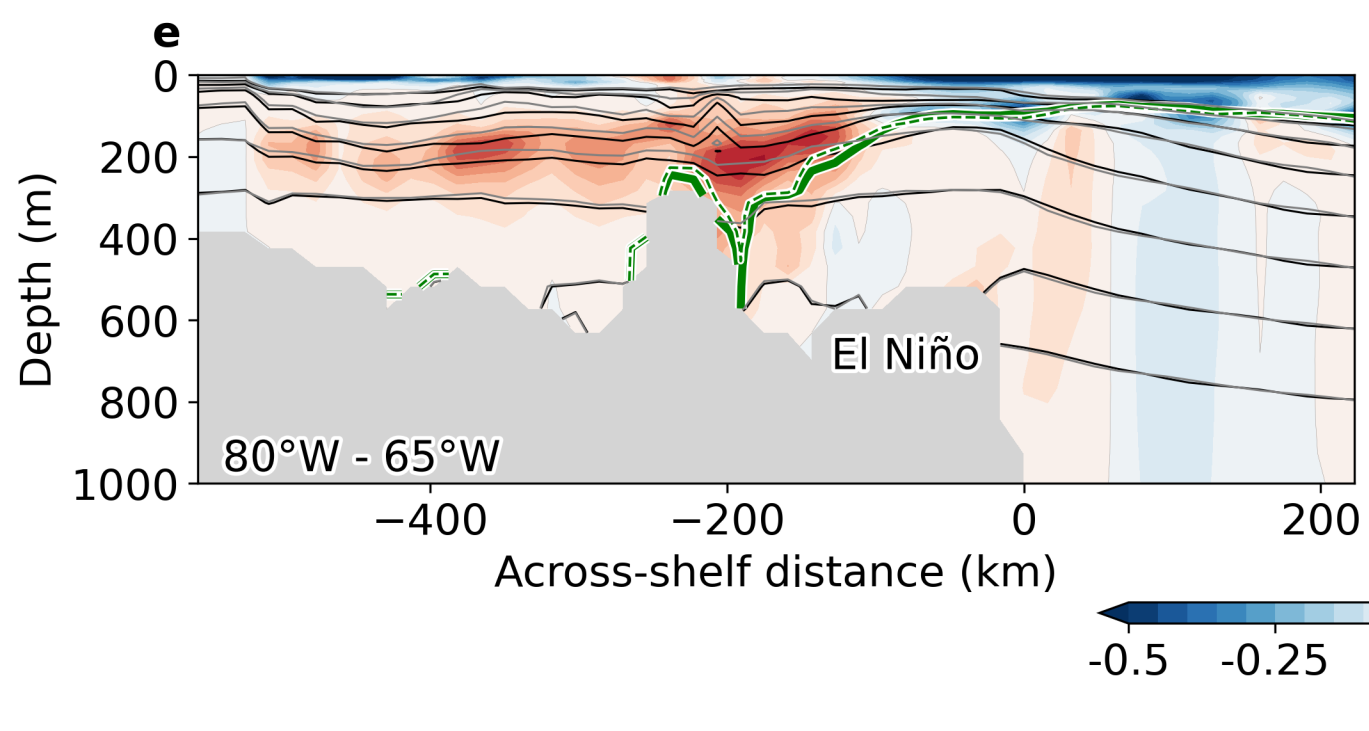
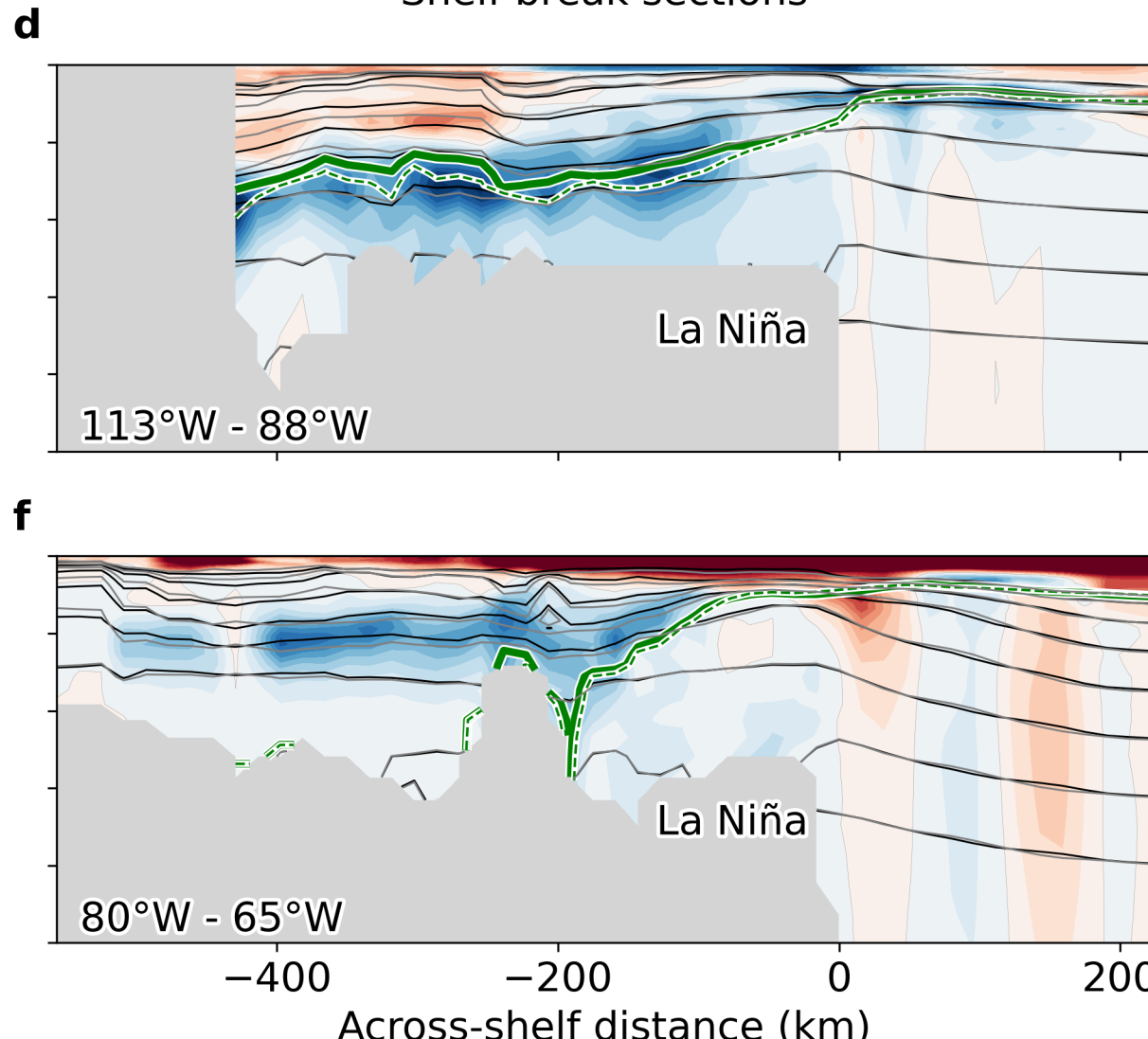
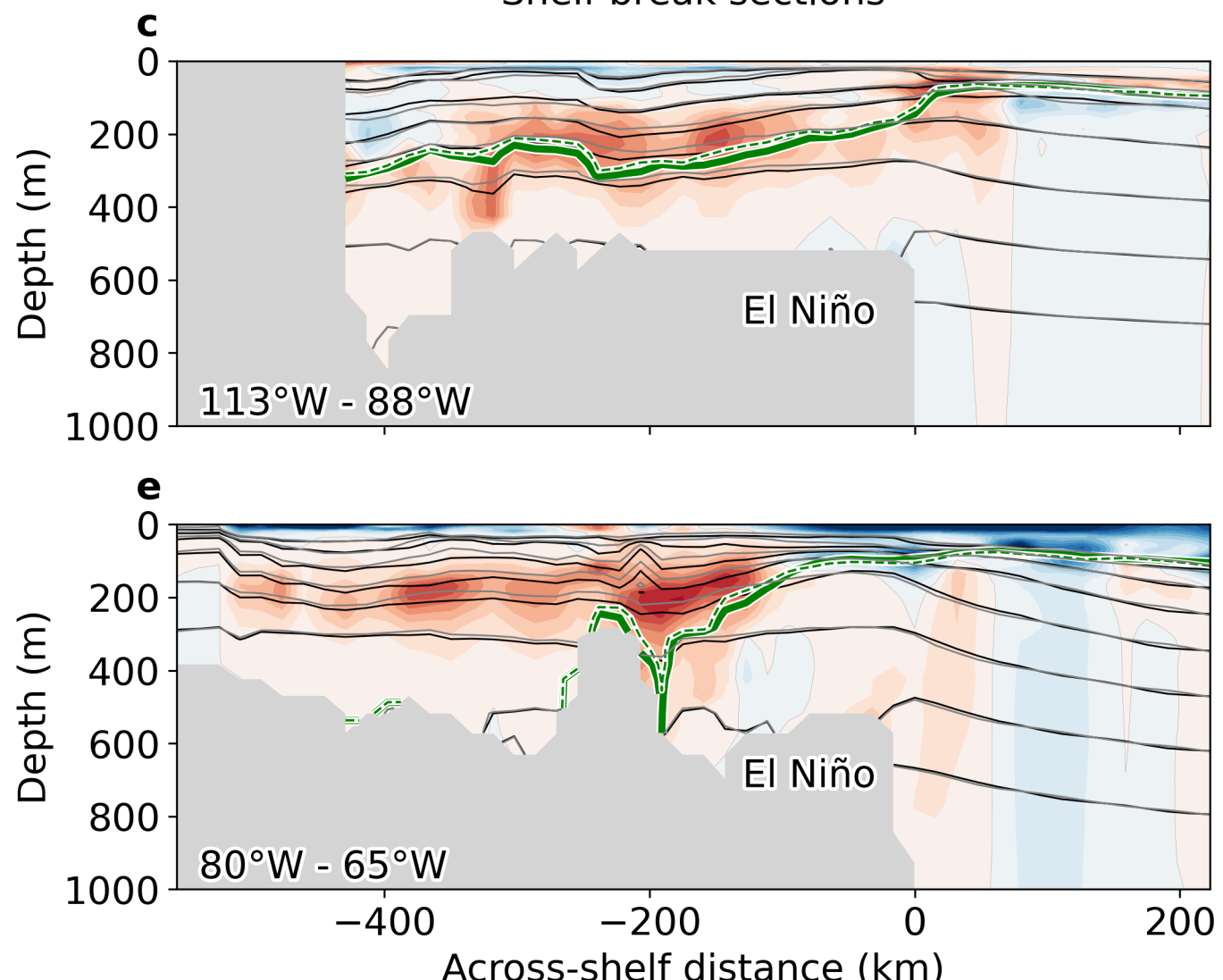
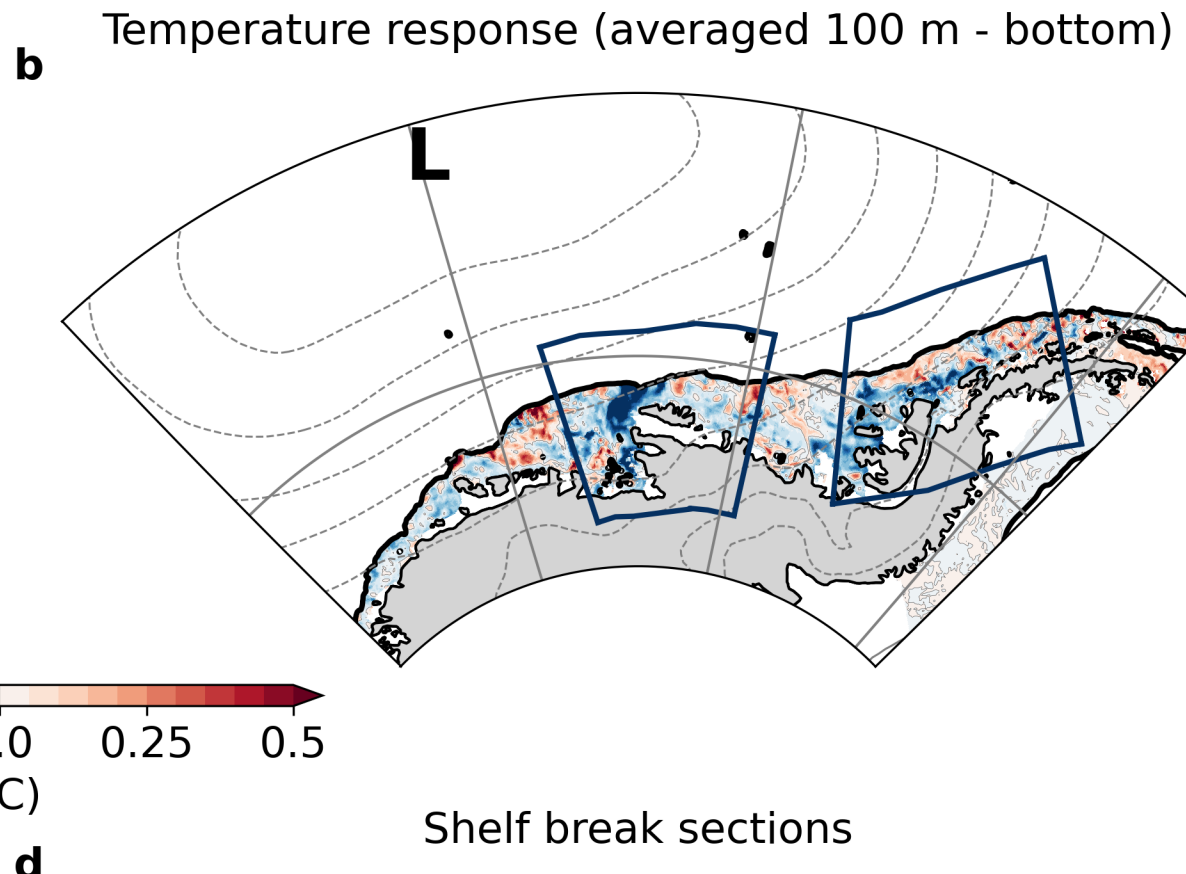
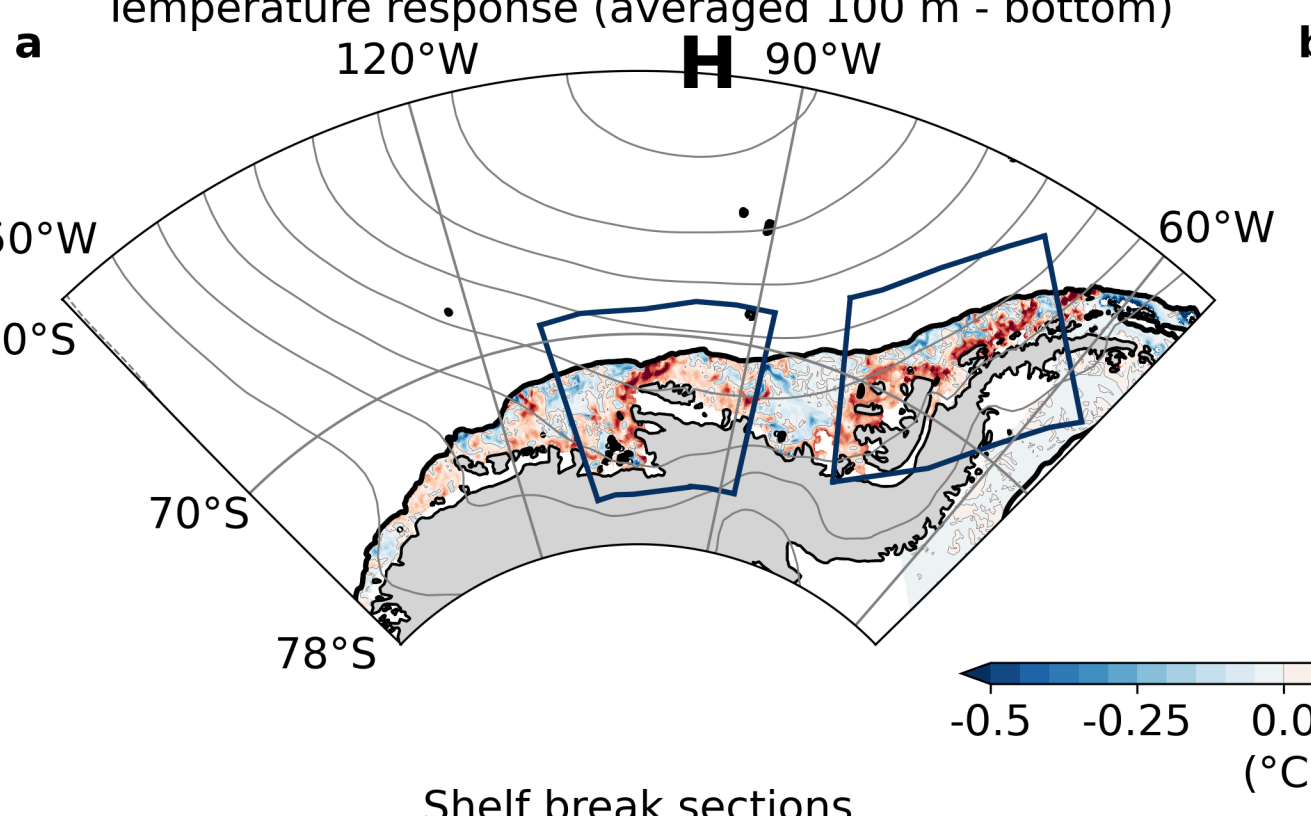
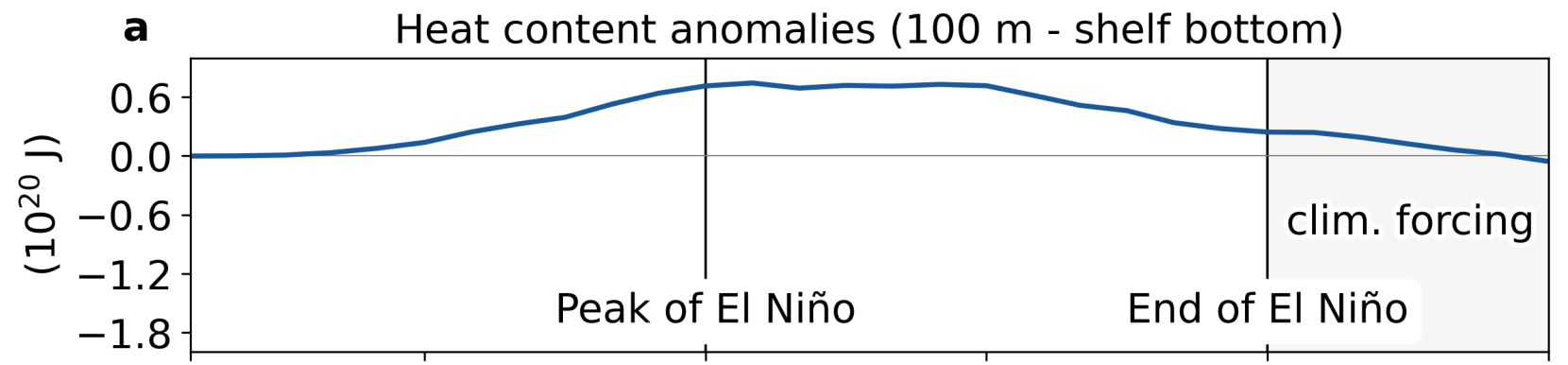
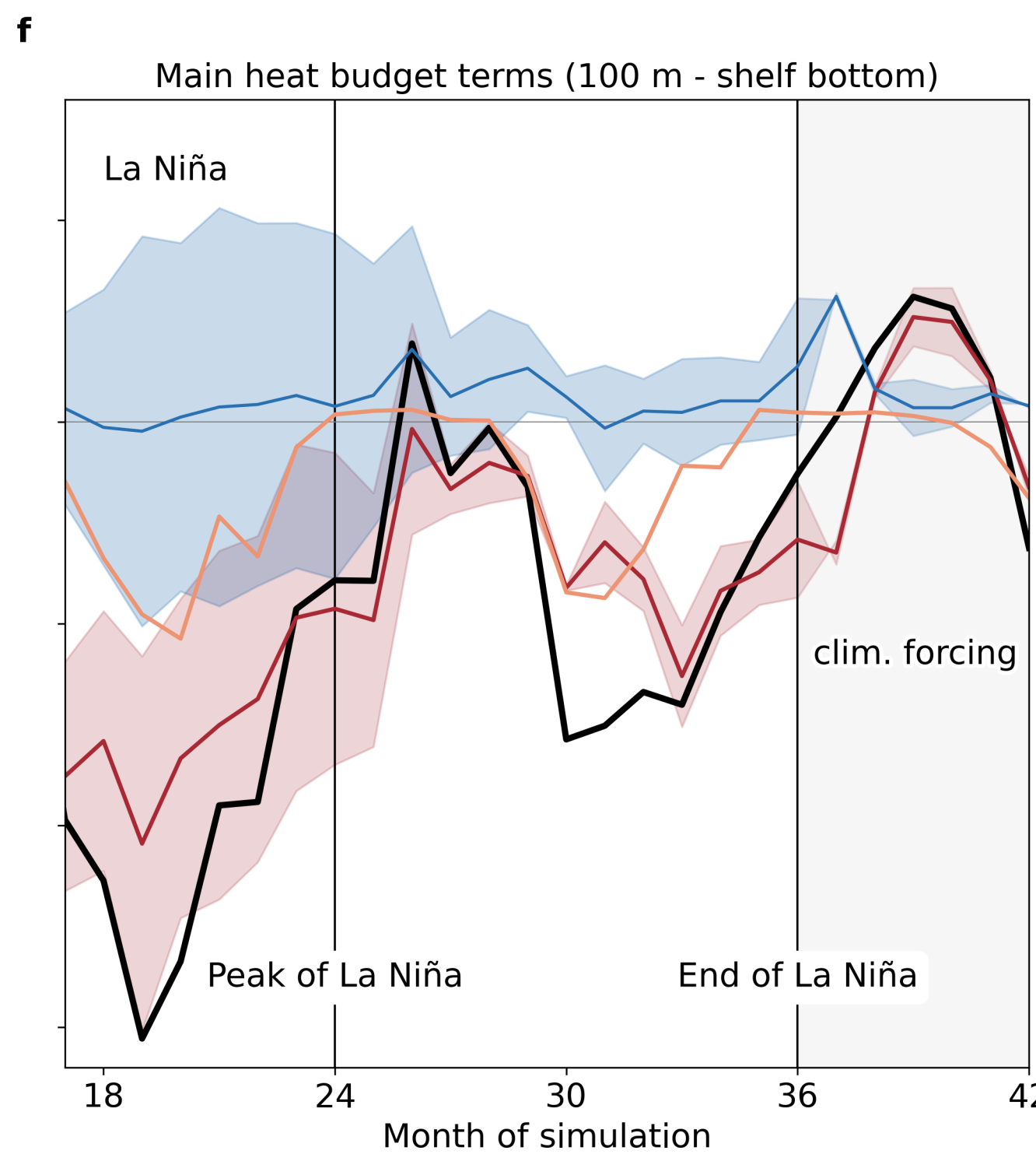
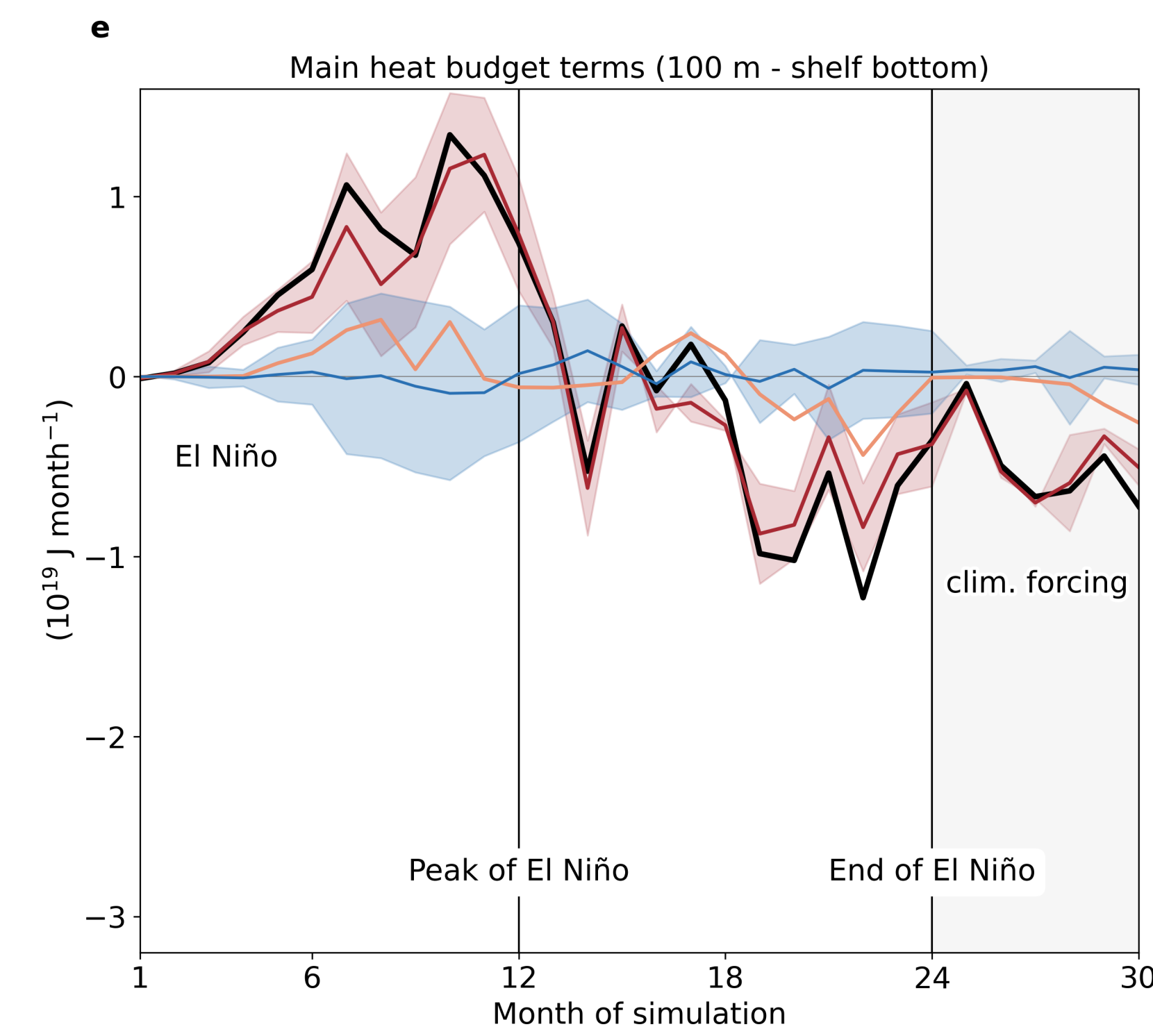
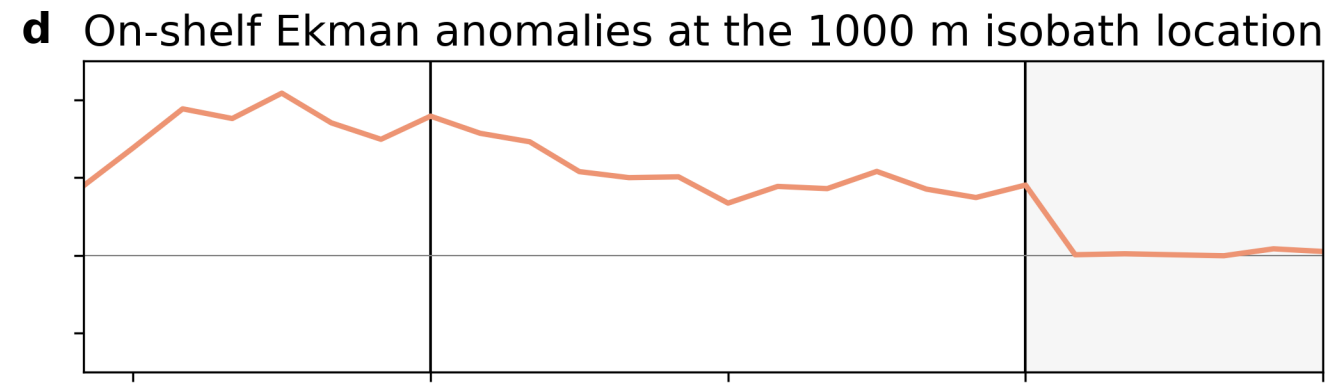
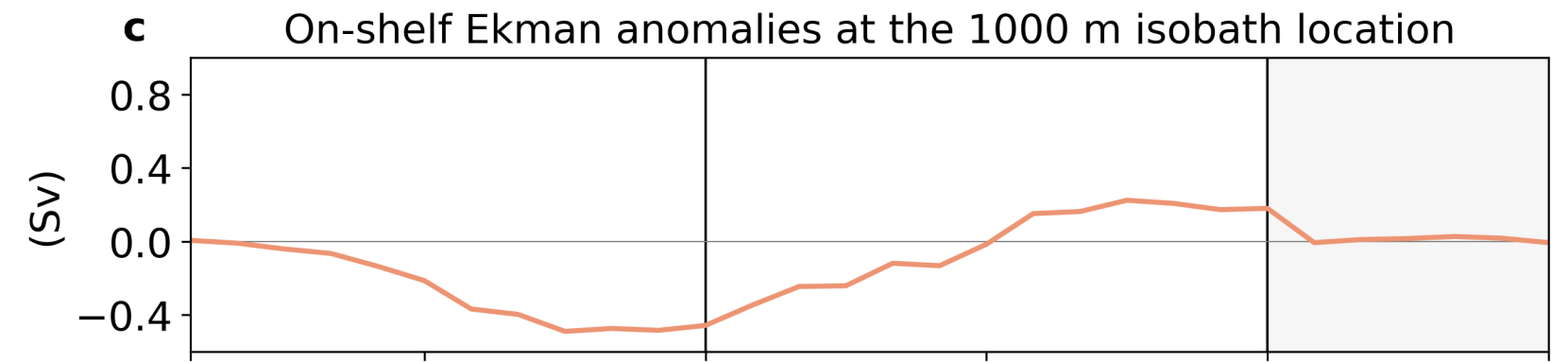
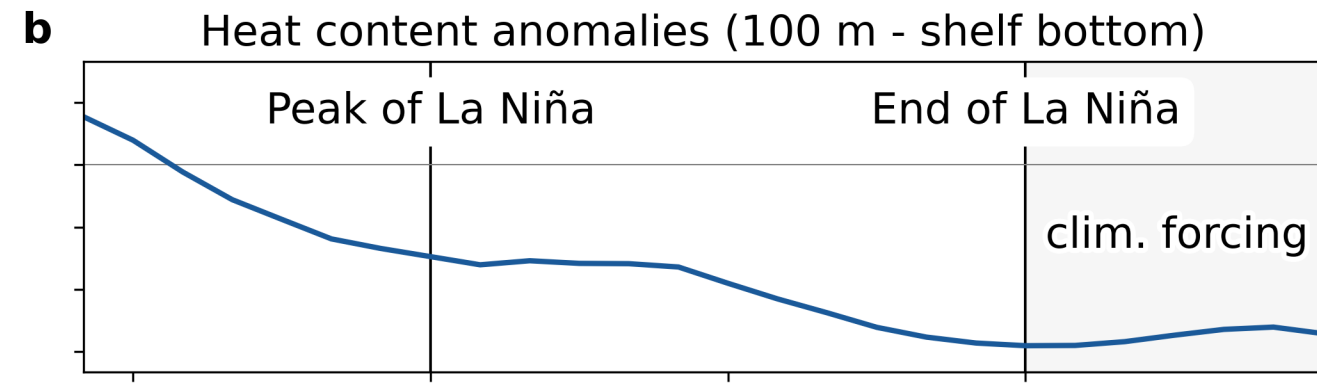


Figure 3.

El Niño simulation



La Niña simulation



— Change in heat content
— Across-shelf heat flux
■ Uncertainty limits of across-shelf heat flux

— Vertical mixing
— Vertical heat flux
■ Uncertainty limits of vertical heat flux

Figure 4.

